Hypoxia truncates and constitutively activates the key cholesterol synthesis enzyme squalene monooxygenase

Hudson W. Coates[1], Ellen M. Olzomer[1], Ximing Du[1], Rhonda Farrell[2,3], Hongyuan Yang[1], Frances L. Byrne[1], and Andrew J. Brown[1]*

[1]School of Biotechnology and Biomolecular Sciences, UNSW Sydney, Sydney NSW 2052, Australia

[2]Chris O'Brien Lifehouse, Camperdown, NSW 2050, Australia

[3]Prince of Wales Private Hospital, Randwick, NSW 2031, Australia

*Corresponding author. Email: aj.brown@unsw.edu.au

Abstract

Cholesterol synthesis is both energy- and oxygen-intensive, yet relatively little is known of the regulatory effects of hypoxia on pathway enzymes. We previously showed that the rate-limiting and first oxygen-requiring enzyme of the committed cholesterol synthesis pathway, squalene monooxygenase (SM), can undergo partial proteasomal degradation that renders it constitutively active. Here, we show that hypoxia is the physiological trigger for this truncation, which occurs through a two-part mechanism: (1) increased targeting of SM to the proteasome *via* stabilization of the E3 ubiquitin ligase MARCHF6, and (2) accumulation of the SM substrate, squalene, which impedes the complete degradation of SM and liberates its truncated form. Truncation of SM permits its localization to lipid droplets and is increased in hypoxic endometrial cancer tissues. These results uncover a feedforward mechanism that enables SM to accommodate fluctuations in substrate levels yet is also a likely contributor to its widely reported oncogenic properties.

Keywords: squalene monooxygenase / cholesterol / hypoxia / proteasome / cancer

Introduction

Cholesterol is an essential component of mammalian cell membranes, yet its aberrant accumulation is detrimental [1]. Most cellular cholesterol arises from an energetically expensive biosynthetic pathway requiring eleven oxygen molecules and over one hundred ATP equivalents per molecule of product [2]. Furthermore, many intermediates of this pathway are toxic in excess [3]. Coordinated regulation of cholesterol synthesis enzymes is therefore vital to ensure that the pathway is active only when required, and that sufficient substrates and cofactors are available to maintain flux through the full length of the pathway.

Squalene monooxygenase (SM, also known as squalene epoxidase or SQLE, EC:1.14.14.17) catalyzes the rate-limiting conversion of squalene to monooxidosqualene in the committed cholesterol synthesis pathway [4]. This reaction is the first of the pathway to require molecular oxygen, with the introduced epoxide group ultimately forming the signature C3-hydroxyl group of cholesterol. SM can also act a second time on monooxidosqualene to produce dioxidosqualene, the precursor of the potent regulatory oxysterol 24(*S*),25-epoxycholesterol [5]. As a flux-controlling enzyme, SM is subject to metabolic regulation at both the transcriptional level *via* sterol regulatory element-binding proteins [6] and the post-translational level *via* ubiquitination and proteasomal degradation [4]. The latter is mediated by the N-terminal regulatory domain of SM (SM-N100), which senses lipid levels in the endoplasmic reticulum (ER) membrane and accelerates or attenuates SM degradation in response to excess cholesterol or squalene, respectively [7, 8]. These reciprocal feedback and feedforward loops thus fine-tune SM activity according to metabolic demand. SM is typically fully degraded by the proteasome; however, incomplete proteolysis produces a truncated form of SM (trunSM) that lacks a large portion of the lipid-sensing SM-N100 domain but retains the full catalytic domain [9]. This renders trunSM cholesterol-resistant and therefore constitutively active. Although truncation is induced by the SM inhibitor NB-598, human cell lines express similar levels of full-length and truncated SM [9]. This points to the existence of an unknown physiological trigger for truncation.

Clarifying the mechanisms of SM regulation is particularly pertinent given the importance of the enzyme, and cholesterol more generally [10], in oncogenesis. Overexpression of the SM gene *SQLE* is associated with greater invasiveness and lethality in breast [11], prostate [12, 13], and pancreatic cancer [14], amongst others. *SQLE* also shares its genomic locus with the oncogene *MYC*, with which it is frequently co-amplified in cancer [11, 15]. Moreover, myc itself transcriptionally upregulates *SQLE* expression [16], while the tumor suppressor protein p53 downregulates its expression [17]. At the protein level, aberrant SM expression is implicated in colorectal cancer progression [18, 19] and the development of both nonalcoholic steatohepatitis and hepatocellular carcinoma [20, 21]. Given its key role in oxygen-dependent cholesterol synthesis, SM may be particularly critical for cancer cell survival during hypoxia, which is common in the poorly vascularized cores of solid tumors and often associated with poor prognosis [22]. In support of this idea, SM inhibition sensitizes breast and colorectal cancer cells to hypoxia-induced cell death [23]. Although hypoxic cells tend to accumulate cholesterol, there are conflicting reports on changes in biosynthetic flux [24–26]. Furthermore, with the notable exception of the early pathway enzyme 3-hydroxy-3-methylglutaryl-CoA reductase (HMGCR) [27], the effects of hypoxia on individual biosynthetic enzymes are unknown. It is also unclear whether these might be perturbed in a tumor context to favor continued cholesterol synthesis and cell proliferation.

Here, we show that hypoxic conditions induce the truncation of SM in a variety of cell lines through a combination of accelerated proteasomal degradation and inhibition of its complete proteolysis. This occurs due to the accumulation of both MARCHF6, the major E3 ubiquitin ligase for SM, and squalene, which impedes SM degradation through a mechanism dependent on the SM-N100 regulatory domain. We also show that trunSM, but not full-length

SM, is capable of partitioning to lipid droplets, and that SM truncation is increased and correlates with the magnitude of hypoxia in endometrial cancer tissues. Taken together, our findings point towards a role for the constitutively active trunSM in adaptations to hypoxic conditions and suggest that it contributes to the oncogenic effects of SM activity.

Results

Oxygen availability regulates SM truncation

We previously showed that SM is post-translationally regulated by both its substrate, squalene, and its pathway end-product, cholesterol [4, 8]. The enzyme also undergoes partial proteasomal degradation of its N-terminus to liberate a truncated protein (trunSM) that is cholesterol-resistant and thus constitutively active (Fig. 1A) [9], although the physiological trigger is unknown. As SM is a rate-limiting enzyme of cholesterol synthesis and catalyzes its first oxygen-dependent reaction, we next tested if SM protein levels are affected by oxygen availability. Incubation of HEK293T cells under hypoxic conditions (1% O_2) stabilized hypoxia-inducible factor-1α (HIF1α; Fig. 1B) and upregulated its target genes *VEGF* and *CA9* (Supplementary Fig. S1A), confirming the induction of a hypoxic response. We also noted a striking increase in SM truncation under these conditions, as indicated by the disappearance of full-length SM and accumulation of trunSM (Fig. 1B). Hypoxia-induced truncation of SM increased over time (Fig. 1C) and with the magnitude of oxygen deprivation (Fig. 1D). Notably, trunSM accumulation was greater under the severely hypoxic conditions characteristic of solid tumors (0.5–2% O_2) than the 'physoxic' conditions experienced by normal human tissues *in situ* (3–7.5% O_2) [28]. This suggested that increased SM truncation is a feature of pathophysiological hypoxia. The net result of hypoxia-induced truncation was a progressive increase in the levels of total SM over time (expressed as the sum of full-length SM and trunSM levels; Supplementary Fig. S1B).

We also surveyed SM levels in a panel of cell lines and found that hypoxia-induced accumulation of trunSM was generalizable to all, although full-length SM levels did not decrease in MDA-MB-231 breast cancer cells (Supplementary Fig. S1C). As HIF1α and hypoxia-inducible factor-2α (HIF2α) transcriptionally regulate the cellular response to hypoxia, we next tested if their activity is required for SM truncation. However, knockdown of *HIF1A* and *HIF2A* gene expression in HEK293T cells had no effect on the hypoxia-induced truncation of SM (Supplementary Fig. S1D, E), ruling out the involvement of these transcription factors and their target genes in the phenomenon.

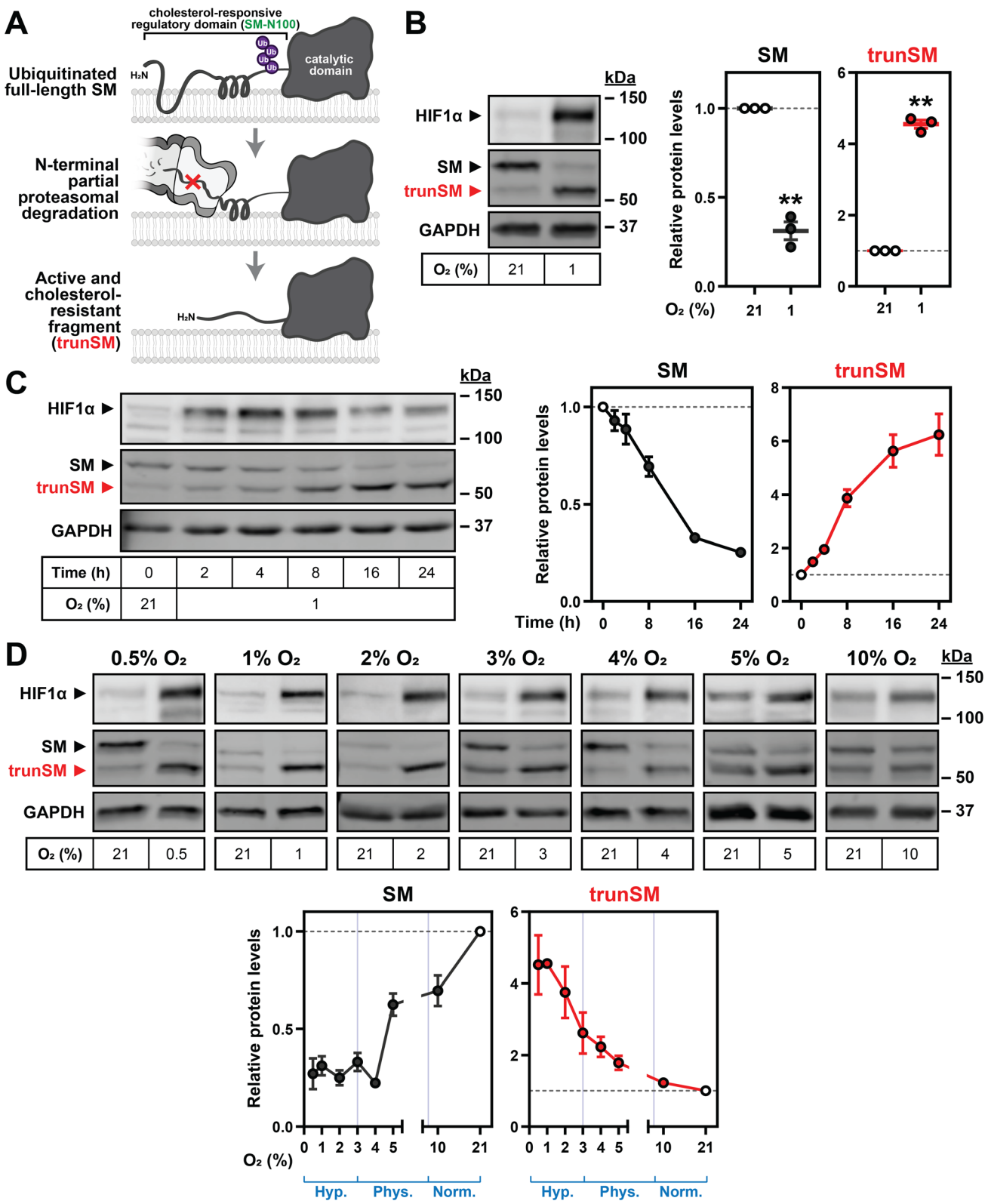

Figure 1. Oxygen availability regulates SM truncation.

(A) Simplified overview of SM truncation [9]. Full-length SM contains an N-terminal domain responsible for feedback regulation by cholesterol. Ubiquitinated SM is targeted to the

proteasome, where proteolysis is prematurely halted within the N-terminal regulatory domain. This liberates a truncated protein (trunSM) that no longer responds to cholesterol and is therefore constitutively active. **(B)** HEK293T cells were incubated under normoxic (21% O_2) or hypoxic (1% O_2) conditions for 24 h. **(C)** HEK293T cells were incubated under normoxic or hypoxic conditions for the indicated times. **(D)** HEK293T cells were incubated under the indicated oxygen concentrations (0.5–21% O_2) for 24 h. **(B–D)** Immunoblotting was performed for SM and truncated SM (trunSM, red). Graphs depict densitometric quantification of protein levels normalized to the normoxic condition, which was set to 1 (dotted line). In (C), oxygen concentrations considered hypoxic (Hyp.), 'physoxic' (Phys.) or normoxic (Norm.) [28] are indicated in blue. Where error bars are not visible, variance is too low to be depicted. Data presented as mean ± SEM from $n \geq 3$ independent experiments (**, $p \leq 0.01$; two-tailed one-sample *t*-test vs. hypothetical mean of 1).

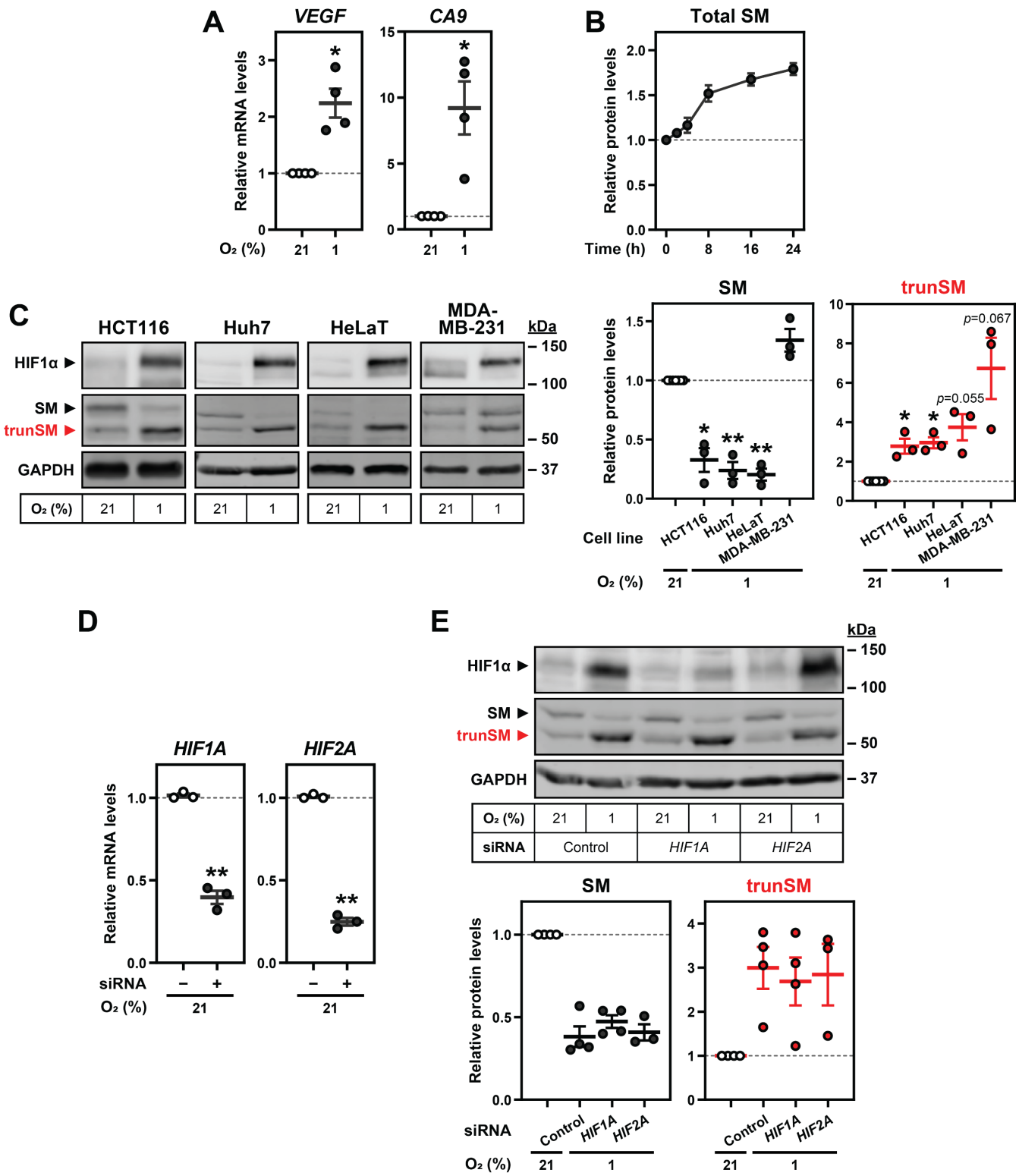

Supplementary Figure S1. Hypoxia-induced truncation of SM is generalizable and independent of hypoxia-inducible factors.

(A) HEK293T cells were incubated under normoxic (21% O_2) or hypoxic (1% O_2) conditions for 24 h. Levels of the indicated HIF1α target gene transcripts were quantified, normalized to

the levels of three housekeeping transcripts and adjusted relative to the normoxic condition, which was set to 1 (dotted line). **(B)** Quantification of total SM levels, expressed as the sum of SM and trunSM levels, in Fig. 1C. **(C)** The indicated cell lines were incubated under normoxic or hypoxic conditions for 24 h. **(D)** HEK293T cells were transfected with the indicated siRNAs for 24 h and incubated under normoxic or hypoxic conditions for 24 h. Levels of siRNA target transcripts in normoxic cells were quantified, normalized to the levels of the *PBGD* housekeeping transcript and adjusted relative to the control siRNA condition, which was set to 1 (dotted line). **(E)** HEK293T cells were treated as described in (B). **(B, C, E)** Graphs depict densitometric quantification of protein levels normalized to the respective normoxic conditions, which were set to 1 (dotted line). **(A–E)** Data presented as mean ± SEM from $n \geq 3$ independent experiments (*, $p \leq 0.05$; **, $p \leq 0.01$; [A, C, D] two-tailed one-sample *t*-test vs. hypothetical mean of 1; [E] two-tailed ratio paired *t*-test vs. control siRNA condition).

139 **Hypoxia transcriptionally and post-translationally reduces full-length SM levels**

140 As the truncation of SM results from its partial proteasomal degradation [9], we
141 reasoned that hypoxia promotes truncation through a two-part mechanism: (1) targeting of full-
142 length SM to the proteasome, and (2) inhibition of its complete degradation. To confirm the
143 first step of this mechanism, we investigated the reason for the decline in full-length SM levels
144 during hypoxia. *SQLE* transcripts were downregulated in hypoxic HEK293T cells, as were
145 transcripts encoding the upstream cholesterol and isoprenoid synthesis enzyme HMGCR
146 (Fig. 2A). Downregulation of *SQLE* transcripts was not observed in MDA-MB-231 cells
147 (Supplementary Fig. S2A), accounting for the unchanged full-length SM levels in this cell line.
148 Although the reduction in *SQLE* and *HMGCR* transcripts in HEK293T cells likely reflected a
149 broad transcriptional suppression of cholesterol synthesis during hypoxia, as reported
150 previously [29, 30], the magnitude of *SQLE* downregulation was unlikely to fully explain the
151 large reduction in SM protein levels (Fig. 1B). Moreover, levels of a constitutively expressed
152 SM construct were markedly reduced during extended hypoxic incubations, with no associated
153 changes in mRNA levels (Fig. 2B, Supplementary Fig. S2B). We concluded that hypoxia
154 reduces the levels of full-length SM through both transcriptional downregulation and
155 accelerated post-translational degradation.

156 The basal and metabolically-regulated degradation of SM occurs through the ubiquitin-
157 proteasome system and is mediated by the SM-N100 regulatory domain [7, 8]. Therefore, we
158 tested the effect of hypoxia on HEK293 cells stably overexpressing an SM-N100 fusion protein
159 (SM-N100-GFP-V5). Like full-length SM, levels of SM-N100-GFP-V5 were reduced under
160 hypoxic conditions (Fig. 2C). Proteasomal inhibition using MG132 rescued SM and
161 SM-N100-GFP-V5 from this reduction, confirming that hypoxia-induced degradation occurs
162 *via* the proteasome. We also noted that the hypoxia-induced accumulation of trunSM was
163 ablated by MG132 (Supplementary Fig. S2C), consistent with the protein arising from partial
164 proteasomal proteolysis of SM [9]. Although hypoxia can trigger autophagy [31], this did not
165 play a role in SM degradation as inhibition of lysosomal acidification using bafilomycin A1
166 had no additive effect with MG132 (Fig. 2C). To identify residues required for hypoxia-
167 induced degradation of SM, we utilized protein constructs with mutations of previously
168 identified ubiquitination sites. Degradation was blunted by the disruption of Lys-82/90/100, a
169 cluster of redundant ubiquitination sites previously found to promote truncation [9], but not by
170 the disruption of Lys-290 [32] (Fig. 2D). Non-canonical cysteine, serine and threonine
171 ubiquitination sites required for the cholesterol-induced degradation of SM [33] also
172 contributed to hypoxia-induced degradation, suggesting that multiple ubiquitin signals are
173 involved.

174 To investigate the mechanism by which hypoxia promotes SM ubiquitination, we
175 considered the possible role of proline hydroxylation. This oxygen-dependent modification,
176 catalyzed by prolyl hydroxylases, is required for the ubiquitination and degradation of HIF1α
177 under normoxic conditions [34], although there is conflicting evidence for the existence of
178 substrates beyond the HIF proteins [35]. Indeed, treatment with prolyl hydroxylase inhibitors
179 had no effect on SM nor SM-N100 levels despite stabilizing HIF1α (Supplementary Fig. S2D).
180 SM and SM-N100 are targeted for proteasomal degradation by the E3 ubiquitin ligase

181 MARCHF6 [36]; therefore, we next tested if increased MARCHF6 activity could account for
182 the hypoxia-induced degradation of SM. In support of this idea, *MARCHF6* knockdown
183 reversed the hypoxic decline in full-length SM levels (Fig. 2E). The relative accumulation of
184 trunSM was also blunted (Supplementary Fig. S2E), consistent with truncation occurring post-
185 ubiquitination by MARCHF6. This effect was not abolished, however, indicating that SM can
186 be truncated even when targeted to the proteasome by other mechanisms. Surprisingly, there
187 was no significant effect of *MARCHF6* knockdown on hypoxia-induced degradation of
188 SM-N100-GFP-V5 (Fig. 2E), suggesting that full-length SM and the isolated SM-N100
189 domain are degraded through different proteasome-dependent routes under these conditions.
190 As truncation involves the full-length protein [9], we elected to further investigate the
191 MARCHF6-mediated regulation of SM.

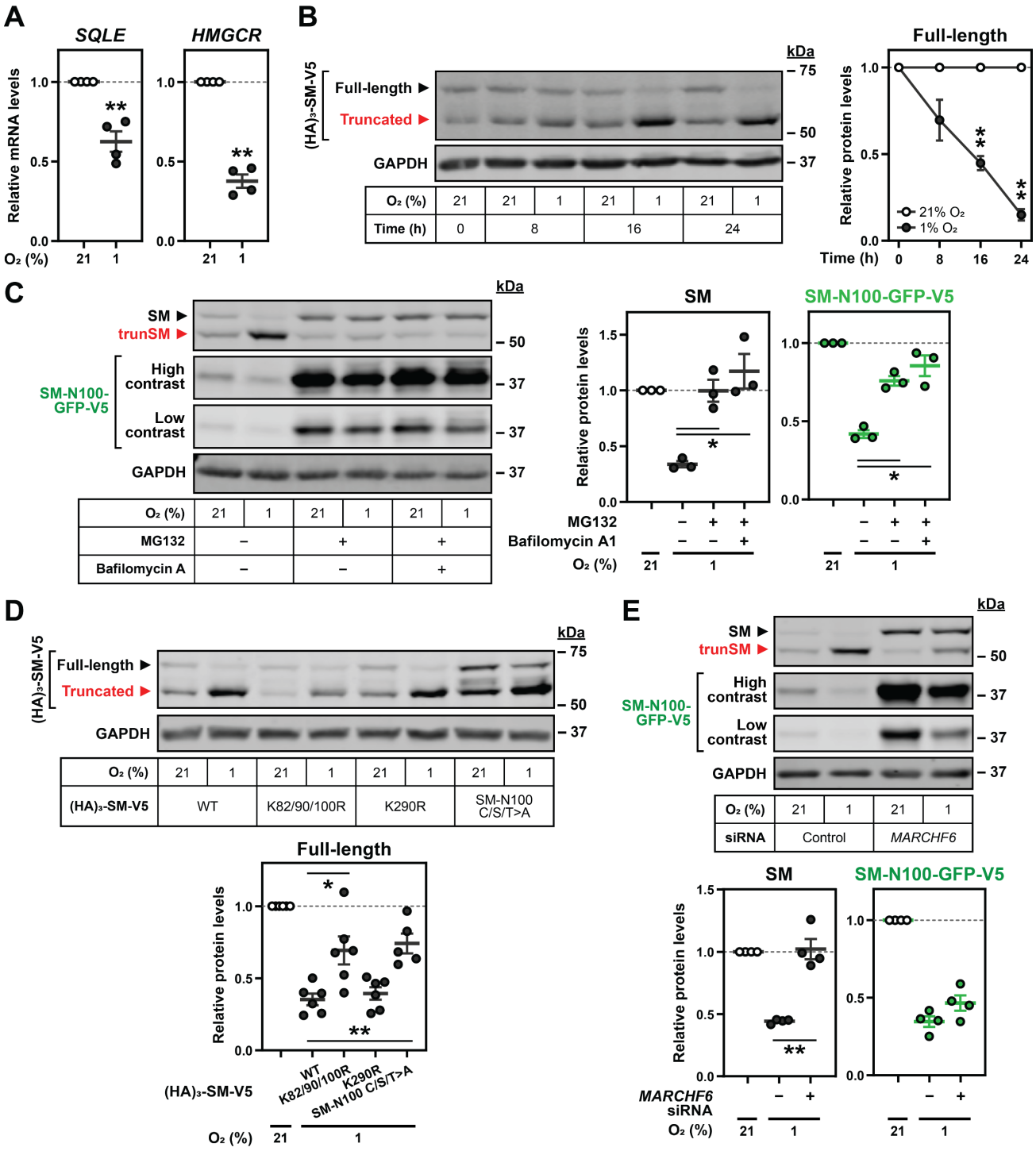

192

193 **Figure 2. Hypoxia transcriptionally and post-translationally reduces full-length SM**
194 **levels.**

195 **(A)** HEK293T cells were incubated under normoxic or hypoxic conditions for 24 h. Levels of
196 the indicated transcripts were quantified, normalized to the levels of three housekeeping
197 transcripts and adjusted relative to the normoxic condition, which was set to 1 (dotted line).
198 **(B)** HEK293T cells were transfected with $(HA)_3$-SM-V5 for 24 h and incubated under

normoxic or hypoxic conditions for the indicated times. **(C)** HEK SM-N100-GFP-V5 cells were treated with or without 20 µM MG132 and 20 nM bafilomycin A1 under normoxic or hypoxic conditions for 16 h. **(D)** HEK293T cells were transfected with the indicated constructs for 24 h and incubated under normoxic or hypoxic conditions for 16 h. **(E)** HEK SM-N100-GFP-V5 cells were transfected with control or *MARCHF6* siRNA for 24 h and incubated under normoxic or hypoxic conditions for 16 h. **(B–E)** Graphs depict densitometric quantification of protein levels normalized to the respective normoxic conditions, which were set to 1 (dotted line). **(A–E)** Data presented as mean ± SEM from $n \geq 3$ independent experiments (*, $p \leq 0.05$; **, $p \leq 0.01$; [A, B] two-tailed one-sample *t*-test vs. hypothetical mean of 1; [C–E] two-tailed ratio paired *t*-test vs. vehicle, wild-type [WT] or control siRNA condition).

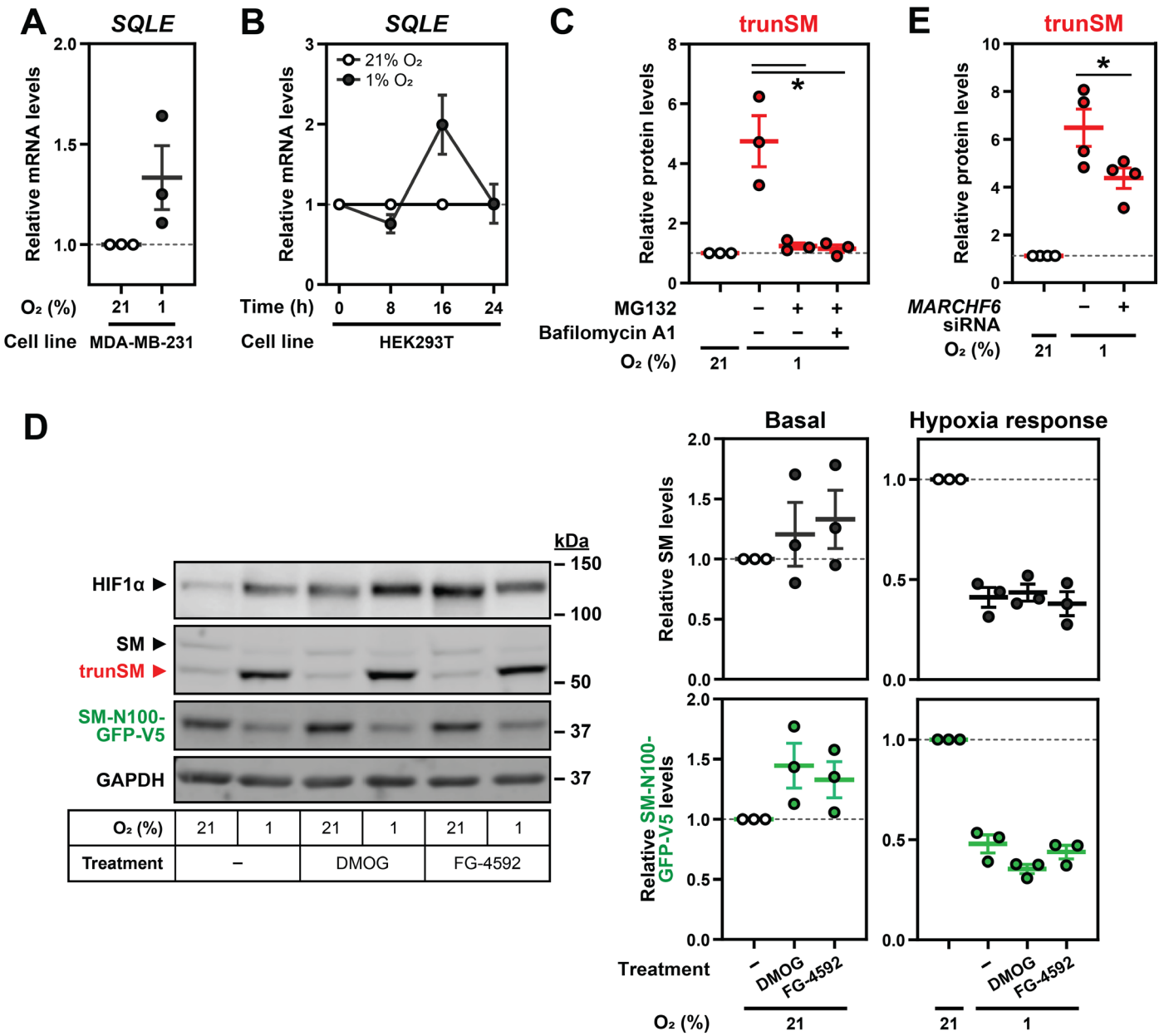

Supplementary Figure S2. Hypoxia-induced degradation of full-length SM is independent of proline hydroxylation.

(A) MDA-MB-321 cells were incubated under normoxic or hypoxic conditions for 24 h. Levels of *SQLE* transcripts were quantified, normalized to the levels of three housekeeping transcripts and adjusted relative to the normoxic condition, which was set to 1 (dotted line). **(B)** HEK293T cells were treated as described in Fig. 2B. Levels of *SQLE* transcripts were quantified, normalized to the levels of three housekeeping transcripts and adjusted relative to the normoxic condition, which was set to 1 (dotted line). **(C)** Quantification of trunSM levels in Fig. 2C. **(D)** HEK SM-N100-GFP-V5 cells were treated with or without 1 mM DMOG or 25 µM FG-4592 under normoxic or hypoxic conditions for 16 h. **(E)** Quantification of trunSM levels in Fig. 2E. **(C–E)** Graphs depict densitometric quantification of protein levels normalized to the respective

222 normoxic conditions, which were set to 1 (dotted line). **(A–E)** Data presented as mean ± SEM
223 from $n \geq 3$ independent experiments (*, $p \leq 0.05$; [A, B] two-tailed one-sample *t*-test vs.
224 hypothetical mean of 1; [C–E] two-tailed ratio paired *t*-test vs. vehicle or control siRNA
225 condition).

226 **Hypoxia stabilizes the E3 ubiquitin ligase MARCHF6**

227 To study MARCHF6 levels in hypoxic cells, we utilized a previously generated
228 HEK293 cell line stably overexpressing a V5-tagged form of the protein. This construct was
229 used due to the poor performance of endogenous MARCHF6 antibodies [37], and also to
230 eliminate any transcriptional contribution to protein levels. We first examined the response of
231 MARCHF6-V5 to hypoxia and found that it accumulated during prolonged hypoxic
232 incubations, correlating with the maximal decline in full-length SM levels (Fig. 3A).
233 Previously, we showed that cholesterol stabilizes MARCHF6 by interfering with its
234 autoubiquitination and proteasomal degradation [37]. To determine if a similar mechanism
235 accounted for the accumulation of MARCHF6 in hypoxia, we treated MARCHF6-V5 cells
236 with CB-5083, an inhibitor of the ER-associated degradation cofactor valosin-containing
237 protein, or the proteasome inhibitor MG132. Both treatments stabilized MARCHF6, with
238 CB-5083 having a greater effect, as described previously [37]. Importantly, both CB-5083 and
239 MG132 blocked the hypoxia-induced accumulation of MARCHF6 (Fig. 3B), consistent with a
240 mechanism involving reduced proteasomal degradation. We also tested the effect of hypoxia
241 on two MARCHF6 mutants: C9A, an inactive variant lacking a functional RING domain [38],
242 or N890A, a variant that is defective in auto-ubiquitination [39]. Both mutants showed reduced
243 accumulation during hypoxia (Fig. 3C), indicating that the effect on wild-type MARCHF6-V5
244 is due to impaired auto-ubiquitination.

245 Given that Asn-890 is required for the accumulation of MARCHF6 during hypoxia, we
246 next considered whether this residue might be modified by asparagine hydroxylation. This is
247 an oxygen-dependent modification known to control processes such as HIF1α target gene
248 transactivation [40] and protein ubiquitination [41]. To determine if a similar mechanism
249 regulates MARCHF6 in hypoxia, we used siRNA to deplete the asparaginyl hydroxylase
250 FIH-1. Although this increased basal MARCHF6-V5 levels and blunted its hypoxia-induced
251 accumulation (Supplementary Fig. S3A, B), confirmatory experiments using the FIH-1
252 inhibitor DM-NOFD [42] did not reproduce the effect (Supplementary Fig. S3C). We
253 concluded that asparagine hydroxylation is unrelated to the reduced autoubiquitination of
254 MARCHF6 in hypoxia, with the true mechanism currently unknown.

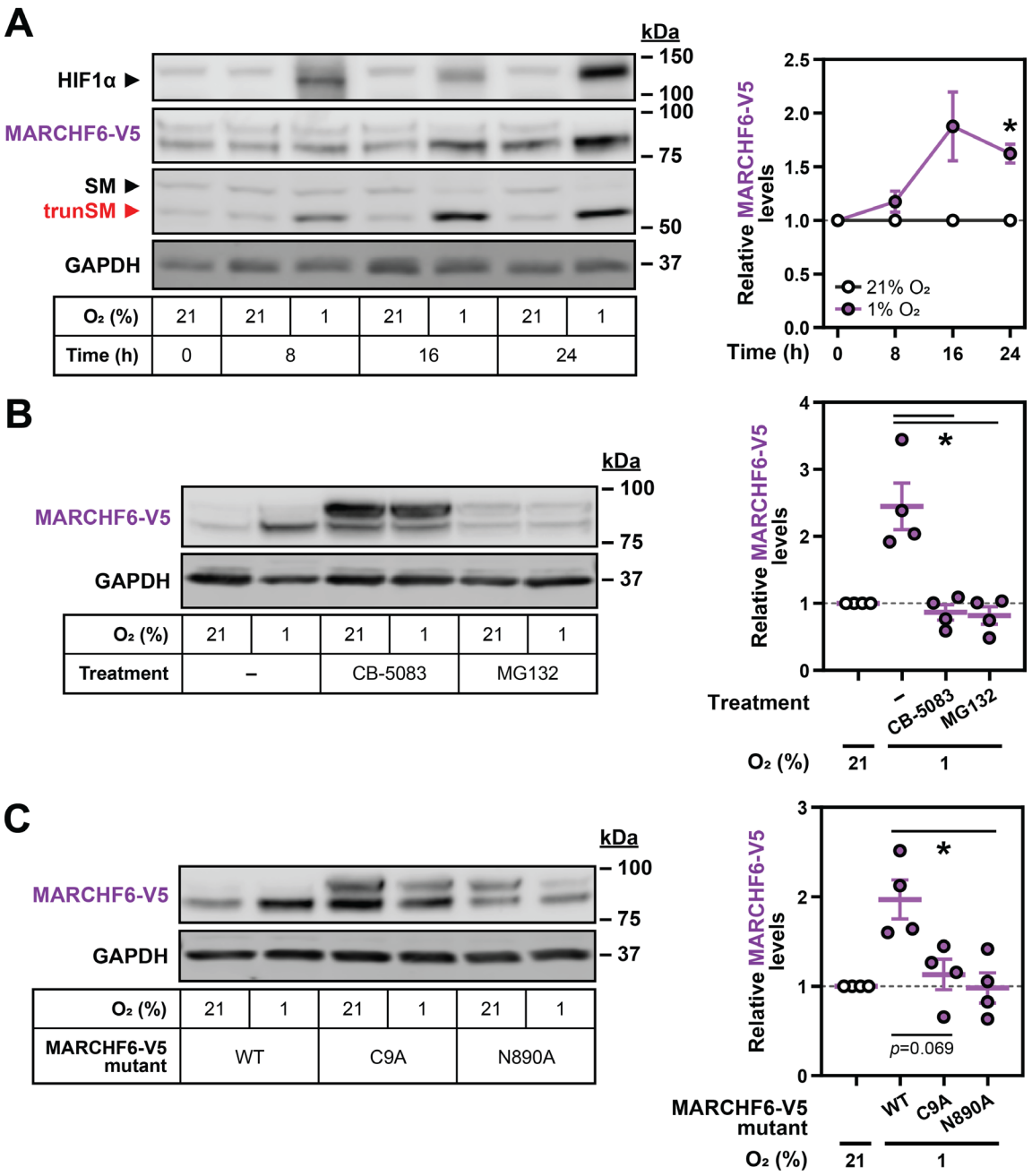

Figure 3. Hypoxia stabilizes the E3 ubiquitin ligase MARCHF6.

(A) HEK MARCHF6-V5 cells were incubated under normoxic or hypoxic conditions for the indicated times. **(B)** HEK MARCHF6-V5 cells were treated with or without 5 µM CB-5083 or 20 µM MG132 under normoxic or hypoxic conditions for 16 h. **(C)** The indicated HEK MARCHF6-V5 cell lines were incubated under normoxic or hypoxic conditions for 16 h. **(A–C)** Graphs depict densitometric quantification of MARCHF6-V5 levels normalized to the respective normoxic conditions, which were set to 1 (dotted line). Data presented as mean ± SEM from $n \geq 3$ independent experiments (*, $p \leq 0.05$; [A] two-tailed one-sample *t*-test vs. hypothetical mean of 1; [B, C] two-tailed ratio paired *t*-test vs. vehicle or WT condition).

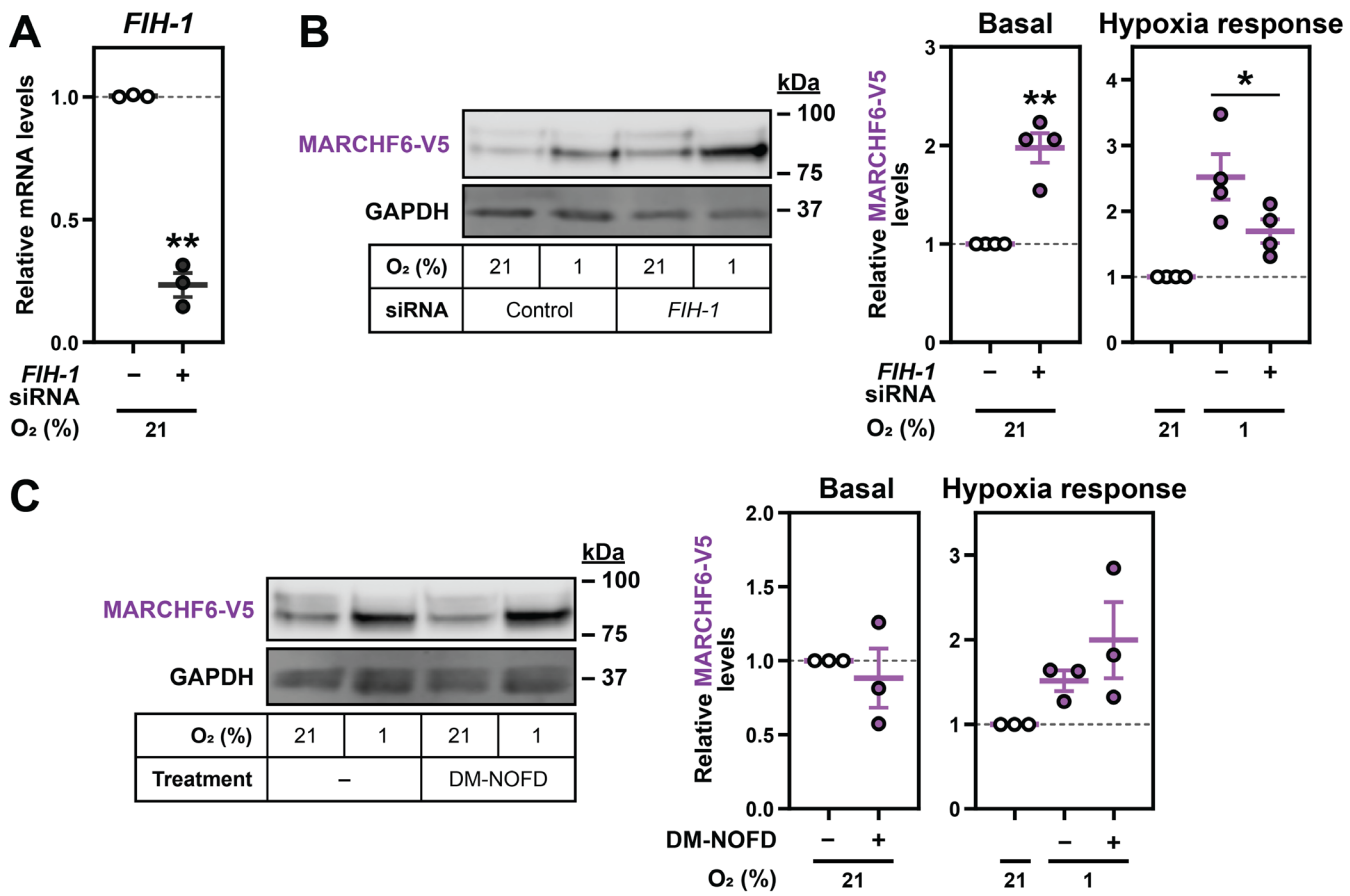

Supplementary Figure S3. Hypoxia-induced stabilization of MARCHF6 is independent of asparagine hydroxylation.

(A) HEK293T cells were transfected with control or *FIH-1* siRNA for 24 h and incubated under normoxic or hypoxic conditions for 24 h. Levels of *FIH-1* target transcripts in normoxic cells were quantified, normalized to the levels of the *PBGD* housekeeping transcript and adjusted relative to the control siRNA condition, which was set to 1 (dotted line). **(B)** HEK MARCHF6-V5 cells were transfected with control or *FIH-1* siRNA for 24 h and incubated under normoxic or hypoxic conditions for 16 h. Graphs depict densitometric quantification of MARCHF6-V5 levels normalized to the (left) vehicle or (right) normoxic condition, which was set to 1 (dotted line). **(C)** HEK MARCHF6-V5 cells were treated with 500 µM DM-NOFD under normoxic or hypoxic conditions for 16 h. **(B, C)** Graphs depict densitometric quantification of MARCHF6-V5 levels normalized to the respective normoxic conditions, which were set to 1 (dotted line). **(A–C)** Data presented as mean ± SEM from $n \geq 3$ independent experiments (*, $p \leq 0.05$; **, $p \leq 0.01$; two-tailed one-sample *t*-test vs. hypothetical mean of 1 or [B, C] two-tailed ratio paired *t*-test vs. control siRNA or vehicle condition).

281 **Hypoxia-induced squalene accumulation promotes partial degradation of SM**

282 Having established that SM undergoes increased proteasomal degradation during
283 hypoxia, we next investigated how low oxygen levels favor its partial rather than complete
284 proteolysis to produce trunSM. As there is extensive precedent for metabolic regulation of
285 cholesterol synthesis enzymes and the pathway contains multiple oxygen-dependent reactions,
286 we considered whether the accumulation of a pathway intermediate might be responsible for
287 this phenomenon. Hypoxia-induced accumulation of trunSM occurred in cells incubated under
288 both lipoprotein-replete and lipoprotein-deficient conditions, in which the cholesterol synthesis
289 pathway is active (Fig. 4A). However, its accumulation was abolished when lipoprotein-
290 deficient cells were co-treated with a statin to inhibit HMGCR and the early cholesterol
291 synthesis pathway. By contrast, there was no effect of sterol depletion on the disappearance of
292 full-length SM. This indicated that an intermediate or end-product of cholesterol synthesis
293 promotes the partial rather than complete degradation of SM during hypoxia. We therefore
294 turned our attention to the SM substrate squalene, given that it allosterically regulates SM
295 degradation [8] and its conversion to monooxidosqualene is the first oxygen-dependent
296 reaction of cholesterol synthesis. Squalene accumulated over the course of a hypoxic
297 incubation (Fig. 4B, Supplementary Fig. S4), consistent with reduced SM activity under low-
298 oxygen conditions. Moreover, this accumulation of squalene was strikingly well-correlated
299 with the previously observed increase in trunSM levels (Fig. 4C), suggesting that the two
300 responses may be linked.

301 Delivery of exogenous squalene mimicked the hypoxia-induced accumulation of
302 trunSM in normoxic HEK293T (Fig. 4D, Supplementary Fig. S5A) and Huh7 cells
303 (Supplementary Fig. S5B), confirming its ability to promote partial degradation of SM.
304 Accumulation of trunSM was also induced by the oxygenated squalene derivatives
305 monooxidosqualene and dioxidosqualene (Fig. 4D) but not by its saturated analogue squalane
306 (Supplementary Fig. S5C), which has similar biophysical properties [43]. This indicated that
307 truncation is promoted by squalene and its structurally related molecules in a specific manner,
308 rather than through bulk membrane effects caused by lipid accumulation. To address the
309 possibility that exogenous squalene is converted to a downstream product responsible for
310 truncation, we performed squalene treatment of *SQLE*-knockout HEK293T cells
311 (Supplementary Fig. S6A–C) transfected with a catalytically inactive SM Y195F mutant [44]
312 to prevent the metabolism of added squalene. The truncated form of the Y195F mutant
313 accumulated upon squalene treatment in *SQLE*-knockout cells, confirming that squalene alone
314 can directly induce truncation (Supplementary Fig. S5D). There was no significant
315 accumulation of the truncated fragment in cells transfected with wild-type SM, likely due to
316 the clearance of exogenous squalene by the overexpressed protein and downstream enzymes.

317 To confirm that endogenously synthesized squalene is sufficient to trigger SM
318 truncation, cells were treated with inhibitors of the relevant cholesterol synthesis enzymes
319 (Supplementary Fig. S5A). The SM inhibitor NB-598 was excluded because of its ability to
320 induce truncation through direct binding and stabilization of the SM catalytic domain that
321 renders it resistant to proteasomal unfolding [8, 45]. Inhibition of squalene synthesis from
322 farnesyl diphosphate (TAK-475) abolished the hypoxia-induced accumulation of trunSM,

323 whereas elevated protein levels were still observed under conditions where squalene remained
324 able to accumulate: inhibition of lanosterol synthesis from monooxidosqualene (BIBB 515), or
325 inhibition of lanosterol demethylation (GR70585X) (Supplementary Fig. S5E). This result
326 confirmed that lanosterol, which also accumulates during hypoxia [27], has no effect on SM
327 truncation. We further noted that the inhibition of squalene or lanosterol synthesis, but not
328 lanosterol demethylation, increased the levels of full-length SM and SM-N100-GFP-V5 under
329 basal conditions. This was in line with our previous finding that farnesyl-containing molecules
330 such as monooxidosqualene, dioxidosqualene and a squalene-derived probe can each stabilize
331 SM *via* its regulatory domain in a similar manner to squalene itself [8]. Interestingly, the basal
332 levels of trunSM were also increased in the presence of these inhibitors (Supplementary
333 Fig. S5E), suggesting that all farnesyl-containing intermediates of cholesterol synthesis are
334 capable of inducing SM truncation. Nevertheless, as the primary substrate of SM, squalene is
335 likely to be the major driver of this process under hypoxic conditions.

336 SM contains two known squalene binding sites: the SM-N100 regulatory domain and
337 the active site of the catalytic domain [8]. As direct binding of the SM inhibitor NB-598 to the
338 catalytic domain results in truncation-promoting stabilization [9], we next considered whether
339 squalene also exerts its effect on truncation through direct binding and stabilization of the
340 catalytic domain. To eliminate the contribution of the SM-N100 domain, we transfected
341 *SQLE*-knockout cells with an ectopic form of trunSM (SM[ΔN65]-V5) that was stabilized by
342 NB-598 (Fig. 4E), consistent with past findings [8, 44]. By contrast, squalene treatment of cells
343 expressing an inactive SM(ΔN65)-V5 mutant (Y195F) did not lead to significant protein
344 stabilization. We concluded that squalene promotes SM truncation *via* the SM-N100 regulatory
345 domain, rather than through direct binding and stabilization of the SM catalytic domain.
346 Squalene treatment also did not increase MARCHF6-V5 levels (Supplementary Fig. S5F),
347 suggesting that the stabilization of the E3 ubiquitin ligase during hypoxia is unrelated to
348 squalene accumulation. This observation was consistent with the hypoxia-induced and
349 MARCHF6-mediated degradation of full-length SM being unaffected by the activity of the
350 cholesterol synthesis pathway (Fig. 4A). Together, this reinforced that squalene exerts its
351 truncation-promoting effects post-ubiquitination, during the proteasomal-degradation of SM.

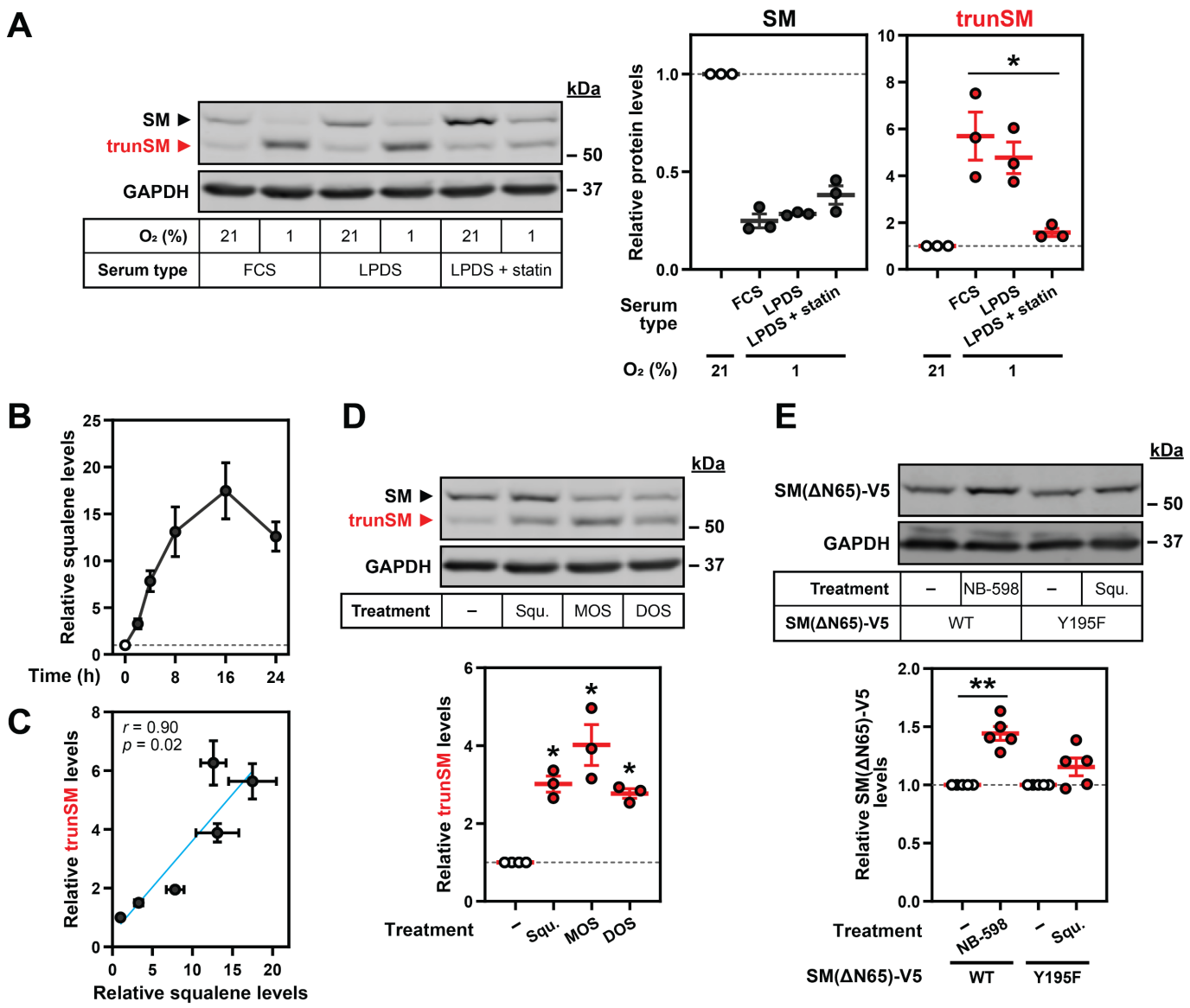

Figure 4. Hypoxia-induced squalene accumulation promotes partial degradation of SM.

(A) HEK293T cells were incubated in medium containing fetal calf serum (FCS), lipoprotein-deficient FCS (LPDS) or LPDS containing 5 µM mevastatin and 50 µM mevalonolactone (LPDS + statin) for 8 h, refreshed in their respective media and incubated under normoxic or hypoxic conditions for 16 h. **(B)** HEK293T cells were incubated under normoxic or hypoxic conditions for the indicated times. Non-saponifiable lipids were extracted, and squalene levels were determined using gas chromatography-mass spectrometry and adjusted relative to the normoxic condition, which was set to 1 (dotted line). The maximal squalene level detected was 0.66 ± 0.12 ng per µg of total protein. **(C)** Pearson correlation between squalene levels in (B) and trunSM levels in Fig. 1C. Blue line indicates linear regression. **(D)** HEK293T cells were treated with or without 300 µM squalene (Squ.), monooxidosqualene (MOS) or dioxidosqualene (DOS) for 16 h. **(E)** HEK293T *SQLE*-knockout (*SQLE*-KO) clone 10 (c10) cells were transfected with the indicated constructs for 24 h, then treated with or without 1 µM

366 NB-598 or 300 µM squalene for 16 h. **(A, D, E)** Graphs depict densitometric quantification of
367 trunSM or truncated protein levels normalized to the (A) respective normoxic conditions or
368 (D, E) respective vehicle conditions, which were set to 1 (dotted line). **(A–E)** Data presented
369 as mean ± SEM from $n \geq 3$ independent experiments (*, $p \leq 0.05$; **, $p \leq 0.01$; [A] two-tailed
370 ratio paired *t*-test vs. FCS condition; [D, E] two-tailed one-sample *t*-test vs. hypothetical mean
371 of 1).

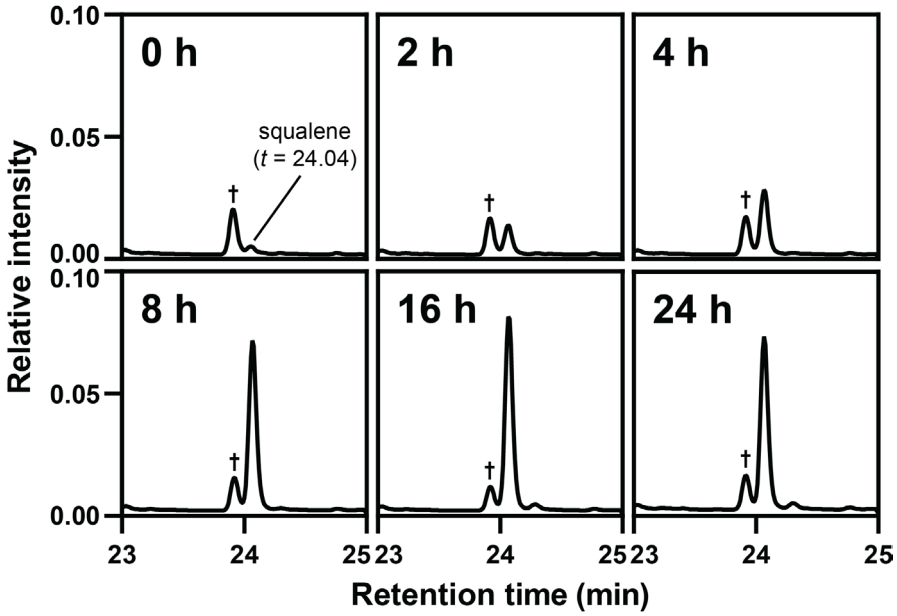

Supplementary Figure S4. Hypoxia induces squalene accumulation.

Representative selective ion monitoring chromatogram traces from gas chromatography-mass spectrometry analysis of squalene levels in Fig. 4B. Abundance was normalized to the 5α-cholestane internal standard, which was set to 1. Dagger indicates a non-specific analyte.

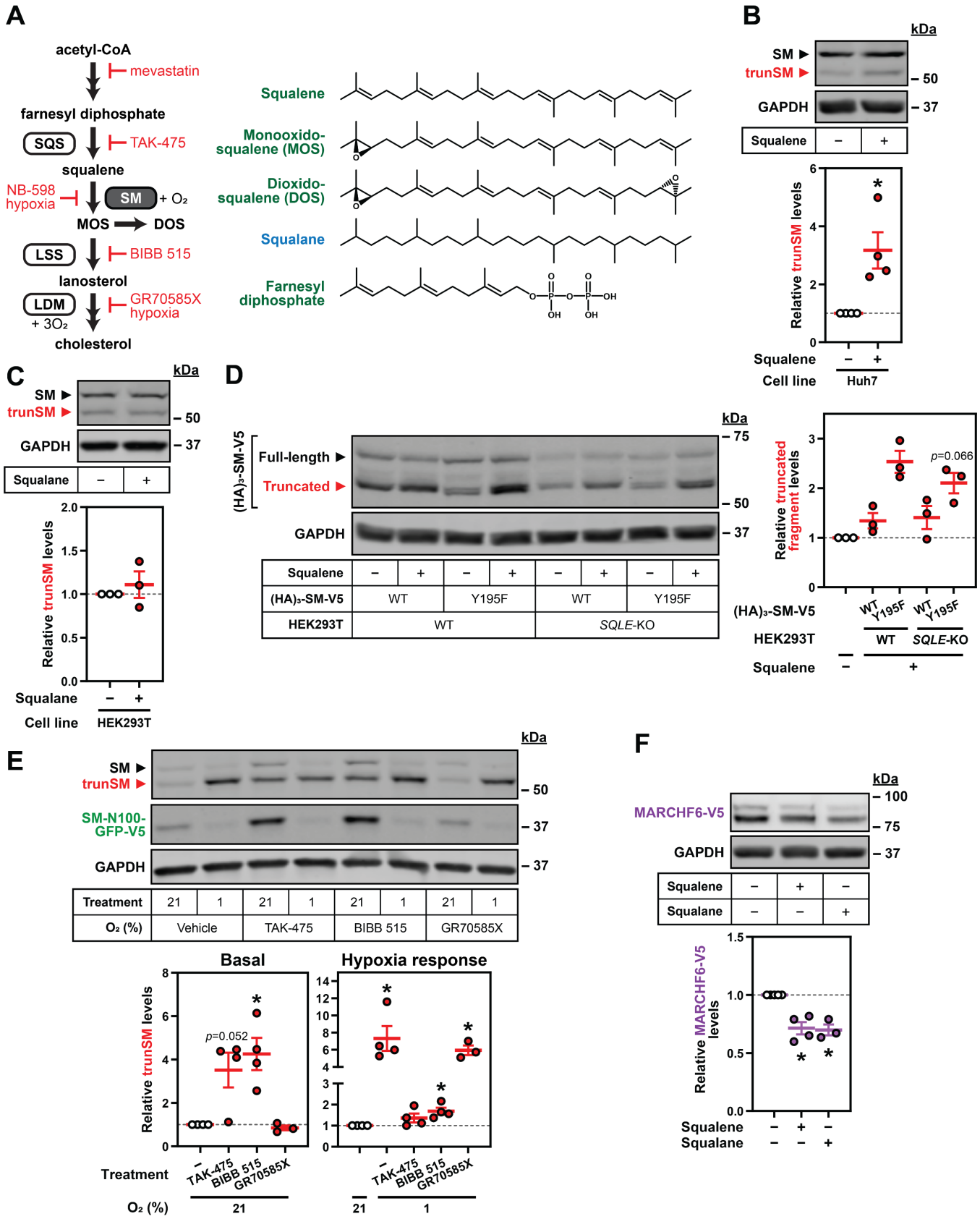
A
acetyl-CoA
mevastatin
farnesyl diphosphate
SQS
TAK-475
squalene
NB-598
hypoxia
SM
+ O₂
MOS
DOS
LSS
BIBB 515
lanosterol
LDM
+ 3O₂
GR70585X
hypoxia
cholesterol
Squalene
Monooxido-squalene (MOS)
Dioxido-squalene (DOS)
Squalane
Farnesyl diphosphate
B
kDa
SM
trunSM
GAPDH
– 50
– 37
Squalene
Relative trunSM levels
Cell line
Huh7
C
Squalane
HEK293T
D
(HA)₃-SM-V5
Full-length
Truncated
– 75
Relative truncated fragment levels
p=0.066
WT
Y195F
SQLE-KO
E
SM-N100-GFP-V5
Treatment
O₂ (%)
Vehicle
TAK-475
BIBB 515
GR70585X
Basal
Hypoxia response
p=0.052
F
MARCHF6-V5
– 100
Relative MARCHF6-V5 levels

377

378 **Supplementary Figure S5. Farnesyl-containing cholesterol synthesis intermediates**
379 **specifically promote partial degradation of SM.**

380 **(A)** Simplified schematic of the cholesterol synthesis pathway depicting activities of squalene
381 synthase (SQS), SM, lanosterol synthase (LSS) and lanosterol 14α-demethylase (LDM),
382 alongside chemical structures of squalene, monooxidosqualene (MOS), dioxidosqualene
383 (DOS), squalane, and farnesyl diphosphate. Double-headed arrows indicate multiple enzymatic
384 steps, red labels indicate inhibitors of cholesterol synthesis, and green and blue labels indicate
385 molecules that were determined to promote or not to promote trunSM accumulation,
386 respectively. **(B)** Huh7 cells were treated with or without 300 µM squalene for 16 h. **(C)**
387 HEK293T cells were treated with or without 300 µM squalane for 16 h. **(D)** Parental (WT) or
388 HEK293T *SQLE*-knockout (*SQLE*-KO) clone 10 (c10) cells were transfected with the indicated
389 constructs for 24 h, then treated with or without 300 µM squalene for 16 h. **(E)** HEK SM-N100-
390 GFP-V5 cells were treated with the indicated compounds under normoxic or hypoxic
391 conditions for 16 h. **(F)** HEK MARCHF6-V5 cells were treated with or without 300 µM
392 squalene or squalane for 16 h. **(B–F)** Graphs depict densitometric quantification of protein
393 levels normalized to the respective vehicle or (E) respective normoxic conditions, which were
394 set to 1 (dotted line). Data presented as mean ± SEM from $n \geq 3$ independent experiments (*,
395 $p \leq 0.05$; two-tailed one-sample *t*-test vs. hypothetical mean of 1).

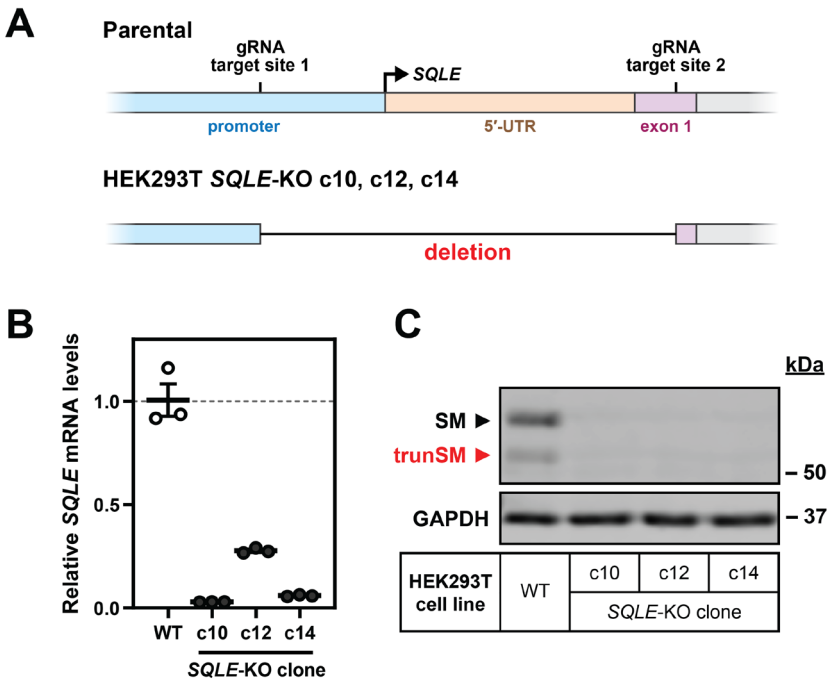

396

397 **Supplementary Figure S6. Generation of *SQLE*-knockout HEK293T cells.**

398 **(A)** HEK293T cells were transfected with CRISPR/Cas9 guide RNAs (gRNAs) targeting the
399 proximal promoter and first exon of the *SQLE* gene as indicated, and three clonal populations
400 of *SQLE*-KO cells were isolated and expanded for each parental cell line. The target region
401 was amplified from genomic DNA and sequenced, which found that all three clones contained
402 a genomic deletion between the gRNA target sites. **(B)** *SQLE* transcript levels were quantified
403 in HEK293T *SQLE*-KO clones, normalized to the *PBGD* housekeeping transcript, and adjusted
404 relative to the parental (WT) cell line, which was set to 1 (dotted line). Data presented as mean
405 ± SEM for technical triplicates from a single experiment. **(C)** Protein lysates from the
406 HEK293T WT cell line and *SQLE*-KO clones were immunoblotted for SM and trunSM.

407 **trunSM uniquely localizes to lipid droplets**

408 Accumulated squalene induces ER stress and is lipotoxic, necessitating its sequestration
409 to lipid droplets [46, 47]. These organelles are also known to form under hypoxic conditions
410 [48], prompting us to examine possible links with trunSM. Several proteomic studies have
411 established that SM localizes to lipid droplets [49–51], but these analyses were unable to
412 distinguish between the full-length and truncated forms of SM. Furthermore, we previously
413 found that trunSM adopts a peripheral rather than integral ER membrane topology, which may
414 improve its compatibility with the lipid droplet monolayer [9]. To expand on these findings,
415 immunofluorescence and lipid droplet staining were used to investigate the localization of the
416 $(HA)_3$-SM-V5 construct in oleate-loaded HeLa cells. The N-terminal $(HA)_3$ tag of the
417 construct, which is present only in the full-length protein (Supplementary Fig. S7A), showed
418 minimal association with the lipid droplet surface (Fig. 5A, C), in contrast to the lipid droplet-
419 localized protein ORP5 (Supplementary Fig. S7B, E) [52]. However, the C-terminal V5 tag,
420 which is present in both the full-length and truncated proteins, was associated with lipid
421 droplets (Fig. 5B, C). The SM(ΔN65)-V5 construct showed a similar association, confirming
422 that the truncated form of SM can partition to lipid droplets. A truncation-resistant
423 $(HA)_3$-SM-V5 mutant (Δ81–120) did not show lipid droplet association of its N- nor C-terminal
424 tags (Supplementary Fig. S7C–E), further demonstrating that full-length SM is excluded from
425 this compartment. Finally, we examined the localization of the SM-N100-GFP-V5 construct,
426 which contains a membrane-embedded re-entrant loop eliminated by truncation [9]. This
427 construct also did not associate with lipid droplets (Fig. 5B, C; Supplementary Fig. S7B, E),
428 indicating that the SM-N100 re-entrant loop is responsible for retaining full-length SM in the
429 ER.

430 As an orthogonal approach to confirm the lipid droplet association of trunSM, we also
431 fractionated lysates from oleate-loaded cells and performed immunoblotting. Consistent with
432 our immunofluorescence data, endogenous trunSM, but not full-length SM, was present in the
433 floating lipid droplet fraction alongside the marker protein ABHD5 (Fig. 5D). Likewise, the
434 truncated form of the $(HA)_3$-SM-V5 construct showed a greater partitioning to lipid droplets
435 than its full-length counterpart. In stark contrast, SM-N100-GFP-V5 did not partition to lipid
436 droplets. These results complemented our immunofluorescence approach and confirmed that
437 the loss of the SM-N100 re-entrant loop renders trunSM uniquely capable of localization to
438 lipid droplets.

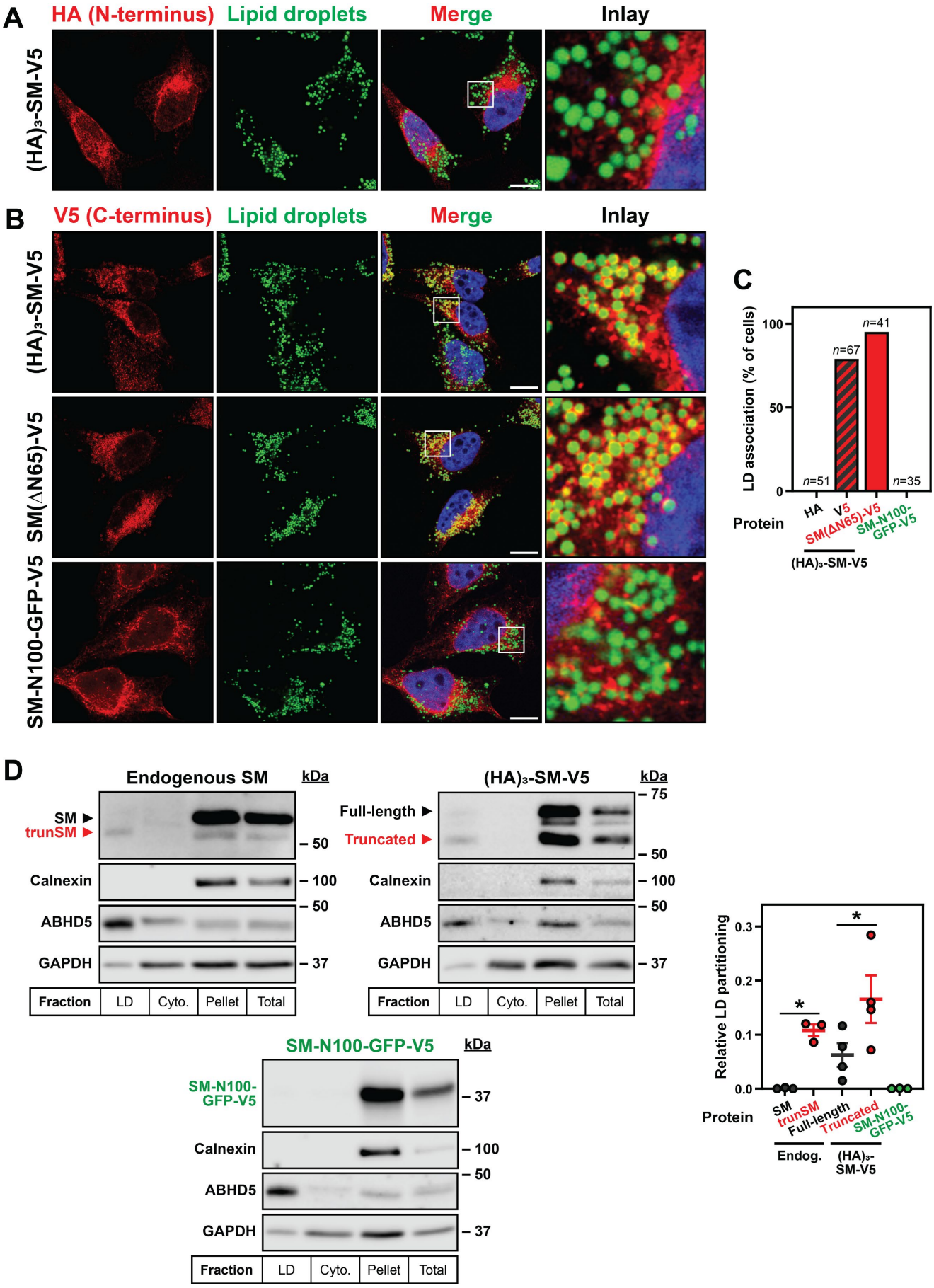
A
HA (N-terminus)
Lipid droplets
Merge
Inlay
(HA)3-SM-V5
B
V5 (C-terminus)
Lipid droplets
Merge
Inlay
(HA)3-SM-V5
SM(ΔN65)-V5
SM-N100-GFP-V5
C
LD association (% of cells)
100
50
0
n=51
n=67
n=41
n=35
Protein
HA
V5
SM(ΔN65)-V5
SM-N100-GFP-V5
(HA)3-SM-V5
D
Endogenous SM
kDa
SM
trunSM
50
Calnexin
100
50
ABHD5
GAPDH
37
Fraction
LD
Cyto.
Pellet
Total
(HA)3-SM-V5
kDa
Full-length
Truncated
75
50
Calnexin
100
50
ABHD5
GAPDH
37
Fraction
LD
Cyto.
Pellet
Total
SM-N100-GFP-V5
kDa
SM-N100-GFP-V5
37
Calnexin
100
50
ABHD5
GAPDH
37
Fraction
LD
Cyto.
Pellet
Total
Relative LD partitioning
0.3
0.2
0.1
0.0
*
*
Protein
SM
trunSM
Full-length
Truncated
SM-N100-GFP-V5
Endog.
(HA)3-SM-V5

439

440 **Figure 5. trunSM uniquely localizes to lipid droplets.**

441 HeLa cells were transfected with the indicated constructs for 24 h and treated with 300 µM
442 oleate-bovine serum albumin complexes for 16 h. **(A, B)** Cells were fixed, lipid droplets (LDs)
443 were stained with BODIPY 493/503, and (A) anti-HA or (B) anti-V5 immunofluorescence was
444 performed (scale bar: 10 µm). **(C)** Quantification of LD association in (A) and (B), expressed
445 as the percentage of imaged transfected cells (*n*) with LD-proximal localization of the protein
446 and epitope of interest. Data were collected across two independent experiments. **(D)** LD,
447 cytosol (Cyto.), pellet, and total fractions were collected and adjusted for protein content, and
448 immunoblotting was performed for calnexin (endoplasmic reticulum marker), ABHD5 (LD
449 marker), and GAPDH (cytosol marker). Graph depicts quantification of LD partitioning,
450 expressed as the ratio between protein levels in LD and membrane fractions normalized to that
451 of ABHD5. Data presented as mean ± SEM from $n \geq 3$ independent experiments (*, $p \leq 0.05$;
452 two-tailed ratio paired *t*-test vs. full-length endogenous [endog.] SM or full-length $[HA]_3$-SM-
453 V5).

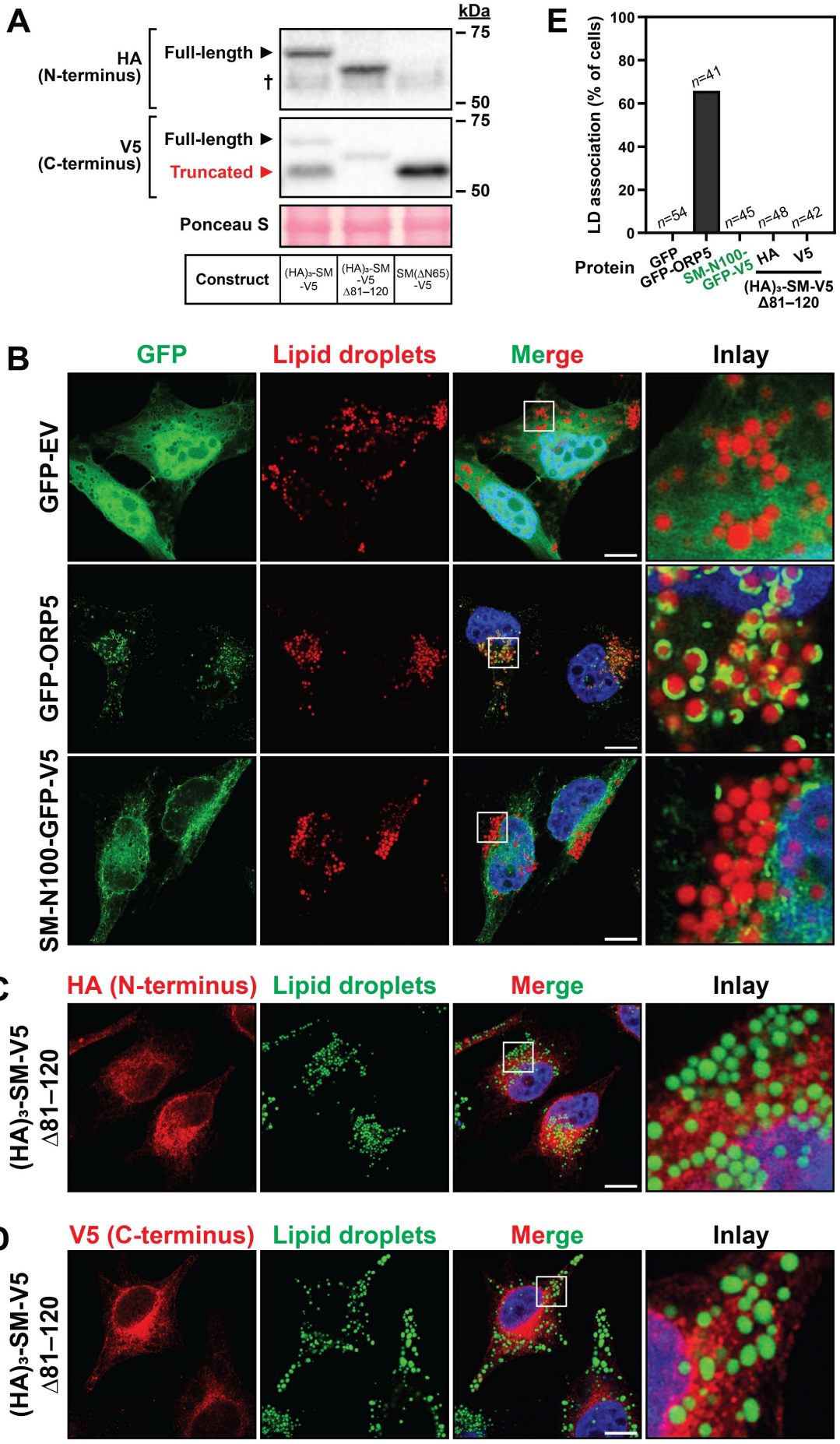
A
kDa
HA
(N-terminus)
Full-length
†
– 75
– 50
V5
(C-terminus)
Full-length
Truncated
– 75
– 50
Ponceau S
Construct
(HA)3-SM -V5
(HA)3-SM -V5 Δ81–120
SM(ΔN65) -V5
E
LD association (% of cells)
100
80
60
40
20
0
n=54
n=41
n=45
n=48
n=42
Protein
GFP
GFP-ORP5
SM-N100-GFP-V5
HA
V5
(HA)3-SM-V5 Δ81–120
B
GFP
Lipid droplets
Merge
Inlay
GFP-EV
GFP-ORP5
SM-N100-GFP-V5
C
HA (N-terminus)
Lipid droplets
Merge
Inlay
(HA)3-SM-V5 Δ81–120
D
V5 (C-terminus)
Lipid droplets
Merge
Inlay
(HA)3-SM-V5 Δ81–120

454

455 **Supplementary Figure S7. Non-truncated SM does not associate with lipid droplets.**

456 HeLa cells were transfected with the indicated constructs for 24 h and treated with 300 µM
457 oleate-bovine serum albumin complexes for 16 h. **(A)** Immunoblotting was performed for
458 N-terminal $(HA)_3$ and C-terminal V5 tags. Dagger indicates a non-specific band. **(B)** Cells were
459 fixed and lipid droplets (LDs) were stained with LipidTOX Deep Red (scale bar: 10 µm). **(C,**
460 **D)** Cells were fixed, LDs were stained with BODIPY 493/503, and (C) anti-HA or (D) anti-V5
461 immunofluorescence was performed (scale bar: 10 µm). **(E)** Quantification of LD association
462 in (B–D), expressed as the percentage of imaged transfected cells (*n*) with LD-proximal
463 localization of the protein and epitope of interest. Data were collected across two independent
464 experiments.

465 **SM truncation is increased in hypoxic endometrial cancer tissues.**

466 Aberrant SM expression and activity is an emerging hallmark of numerous
467 malignancies [21, 53], yet the contribution of the constitutively active trunSM to oncogenesis
468 is unknown. Therefore, we performed immunoblotting of paired tumor and adjacent benign
469 tissue lysates from cohorts of lean and obese endometrial cancer patients. This cancer type was
470 selected because of its close links with obesity [54, 55] and signaling by cholesterol-derived
471 estrogens [56], as well as the unstudied status of SM in endometrial cancer. Similar trends were
472 observed across both cohorts (Fig. 6A, Supplementary Fig. S8A–C), and the data were pooled.
473 This showed that levels of HIF1α were increased in tumor tissues compared with adjacent
474 benign tissues (Fig. 6B), consistent with the hypoxic conditions that occur within solid tumors
475 [22]. Total SM levels were reduced in tumor tissues (Fig. 6B), yet this was accompanied by a
476 dramatic increase in the proportion of SM that was truncated (Fig. 6C). Moreover, we observed
477 a striking correlation between HIF1α levels and SM truncation across all tissues (Fig. 6D),
478 further supporting the notion that hypoxia and truncation are linked. These results confirmed
479 that the hypoxia-induced truncation of SM is a physiologically relevant phenomenon in human
480 tissues and may contribute to endometrial tumorigenesis.

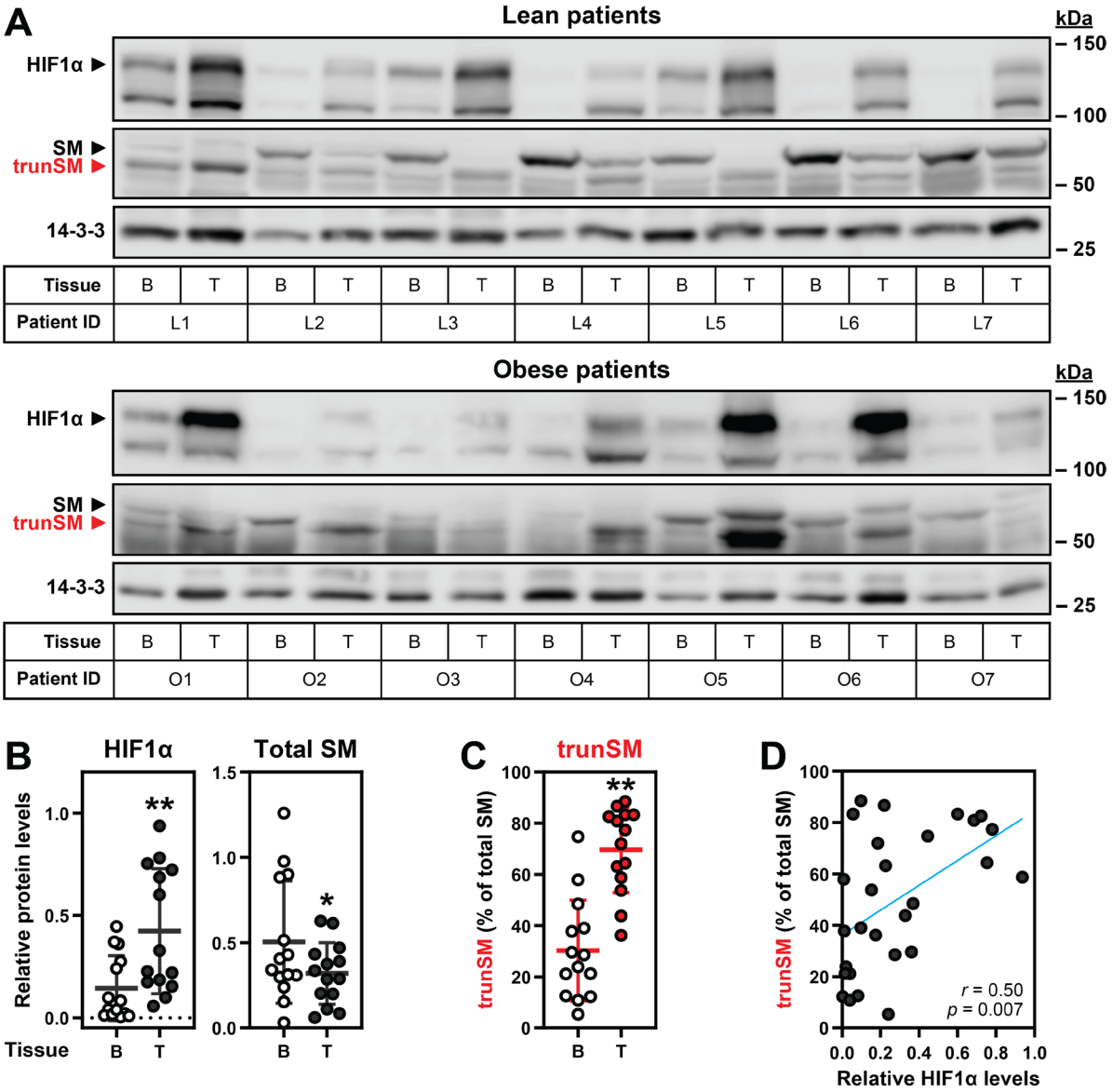

481

482 **Figure 6. SM truncation is increased in hypoxic endometrial cancer tissues.**

483 **(A)** Paired tumor (T) and adjacent benign (B) tissue lysates from lean and obese endometrial
484 cancer patients were analyzed by immunoblotting. **(B, C)** Graphs depict densitometric
485 quantification of protein levels from (A) normalized to the 14-3-3 housekeeping protein, and
486 (C) expressed as a proportion of total SM. Data presented as mean ± SD from $n = 14$ paired
487 tissue sets (*, $p \leq 0.05$; **, $p \leq 0.01$; two-tailed paired *t*-test vs. adjacent benign tissue;
488 normality of distributions confirmed by D'Agostino & Pearson testing [57]). **(D)** Pearson
489 correlation between HIF1α levels in (B) and trunSM levels in (C). Blue line indicates linear
490 regression.

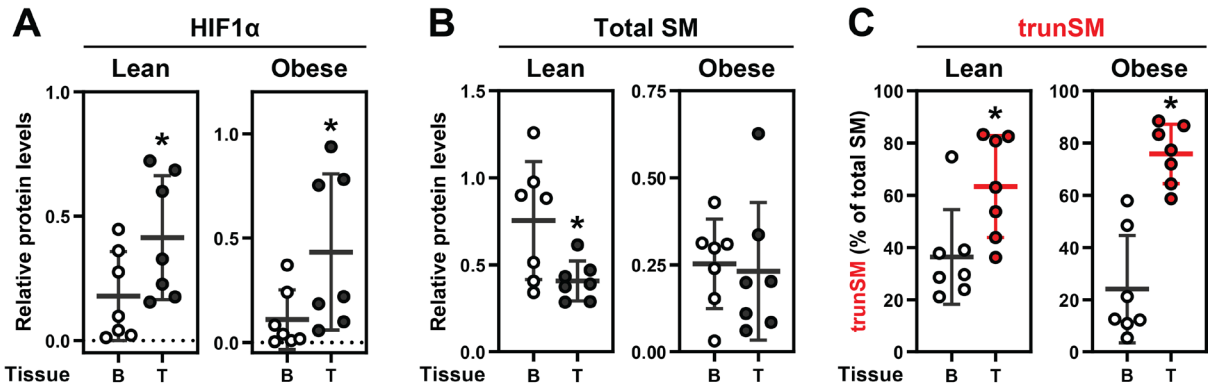

Supplementary Figure S8. SM truncation is increased in endometrial cancer tissues from both lean and obese patients.

Separate quantification of **(A)** HIF1α, **(B)** total SM, and **(C)** trunSM protein levels in tumor (T) and adjacent benign (B) tissues from lean and obese cohorts of endometrial cancer patients in Fig. 6A. Data presented as mean ± SD from $n = 7$ paired tissue sets in each cohort (*, $p \leq 0.05$; two-tailed Wilcoxon matched-pairs signed rank test vs. adjacent benign tissue).

498 # Discussion

499 Cholesterol synthesis is tightly regulated by metabolic supply and demand, with the
500 lipid-sensing and rate-limiting enzyme SM being a key point at which this regulation is exerted.
501 We previously showed that partial proteasomal degradation of SM produces a truncated and
502 constructively active form of the enzyme [9]. In this study, we identified hypoxia as the
503 physiological trigger for trunSM formation in both cell culture and human tissues *in situ*
504 (Fig. 1). Hypoxia-induced truncation occurs through a two-part mechanism: (1) an increase in
505 the levels of MARCHF6, the E3 ubiquitin ligase that targets SM to the proteasome (Fig. 2,
506 Fig. 3), and (2) the accumulation of squalene, which impedes the complete degradation of SM
507 and yields trunSM (Fig. 4). Beyond these mechanistic insights, we found that truncation
508 enables SM to partition to lipid droplets (Fig. 5) and is dramatically increased in endometrial
509 cancer tissues (Fig. 6). Taken together, our results point towards the truncation of SM as an
510 adaptive mechanism to promote squalene clearance during hypoxia, as well as a likely
511 contributor to the widely reported oncogenic properties of SM.

512 **Cholesterol synthesis during hypoxia**

513 Hypoxia places great strain on metabolic processes and necessitates the strict allotment
514 of available oxygen and energy reserves. Cholesterol synthesis is a particularly resource-
515 intensive pathway, requiring eleven oxygen molecules and over one hundred ATP equivalents
516 per molecule of product, yet there are conflicting reports on changes in overall flux from acetyl-
517 CoA to cholesterol during hypoxia [24, 25], indicative of cell type-specific responses.
518 Nevertheless, the small number of studies into individual biosynthetic enzymes indicate that
519 their activity is suppressed by hypoxia at multiple regulatory levels, which is supported by the
520 accumulation of various pathway intermediates [26, 27, 58]. Lanosterol demethylase, which
521 requires three oxygen molecules for catalysis, is transcriptionally downregulated by HIF2α and
522 the hypoxia-induced long non-coding RNA *lincNORS*, contributing to the characteristic
523 accumulation of lanosterol under hypoxic conditions [26, 59]. Lanosterol in turn triggers the
524 ubiquitin-dependent degradation of the early cholesterol synthesis enzyme HMGCR [27],
525 suppressing further oxygen consumption by the pathway. Our study expands this understanding
526 of hypoxic adaptations by establishing that oxygen availability also regulates SM, a rate-
527 limiting enzyme of cholesterol synthesis and the first to require molecular oxygen.

528 We found that SM is transcriptionally downregulated in hypoxic HEK293T cells but
529 not MDA-MB-231 cells, consistent with previously reported cell-type specific changes in
530 *SQLE* expression [23]. This accounted in part for the decline in full-length SM levels, although
531 reduced *SQLE* translation through mechanisms such as mTOR suppression [60] cannot be ruled
532 out as a contributing factor. We also found that, like HMGCR, the translated SM protein is
533 targeted for proteasomal degradation during hypoxia. However, in stark contrast to HMGCR,
534 the net effect of SM degradation under these conditions is the maintenance of, or even an
535 increase in, the number of enzyme molecules available for catalysis. This is due to the increased
536 partial proteolysis of SM to form trunSM, which lacks degron features within the SM-N100
537 regulatory domain and has a dramatically extended half-life yet remains catalytically active

538 [9]. Disruption of the SM-N100 domain also renders trunSM resistant to cholesterol-induced
539 degradation, which is an key element in the metabolic regulation of full-length SM [4, 9].
540 Therefore, the hypoxia-induced truncation of SM ensures that total enzyme levels remain
541 constant even under cholesterol-replete conditions that would typically reduce its abundance.

542 The most plausible explanation for the seemingly paradoxical stabilization of SM
543 during hypoxia is that this can compensate for reduced oxygen availability and allow enzyme
544 activity to be maintained (Fig. 7). There are numerous ways in which the truncation and
545 constitutive activity of SM is beneficial. During transient or low-level hypoxia, it may enable
546 continued cholesterol synthesis so that cell growth and survival is not compromised by the
547 oxygen shortfall. In support of this idea, hypoxia-induced cell death is exacerbated by SM
548 inhibition [23]. Furthermore, the longevity of trunSM is likely to enable rapid resumption of
549 pathway activity when normal oxygen levels are restored. During long-term or severe hypoxia,
550 where there is insufficient oxygen for flux through downstream cholesterol synthesis, the role
551 of trunSM in hypoxia may shift towards the efficient clearance of squalene. While generally
552 considered an inert intermediate, excess squalene induces ER stress and is generally toxic in
553 cells lacking SM activity [47]. A secondary effect of squalene clearance is its downstream
554 conversion to lanosterol, which promotes the shutdown of cholesterol synthesis *via* HMGCR
555 degradation. This mechanism may explain why squalene accumulation lags behind that of
556 lanosterol during the acute phase of hypoxia [27, 58]. Although we detected increased squalene
557 levels at early hypoxic timepoints, a previous study of sterol-depleted cells did not [27], which
558 is likely attributable to the basal upregulation of SM expression under these conditions.
559 Elevated SM activity during hypoxia may also favor the synthesis of dioxidosqualene and
560 ultimately 24(*S*),25-epoxycholesterol, a potent suppressor of cholesterol accretion [61].
561 However, this oxysterol is yet to be studied in a low-oxygen context.

562 **Molecular mechanism of truncation**

563 The first step of SM truncation is its delivery to the proteasome [9]. This is enhanced
564 during hypoxia by a novel ubiquitin signal at the Lys-82/90/100 cluster, as well as the
565 accumulation of the E3 ubiquitin ligase MARCHF6, which facilitates the basal and
566 metabolically-regulated degradation of SM [36]. Non-canonical ubiquitination sites required
567 for cholesterol-induced degradation of SM [33] also contribute to its hypoxic degradation,
568 which can be reconciled by the combination of increased MARCHF6 levels and the sterol-
569 replete conditions under which these experiments were performed. Hypoxic accumulation of
570 MARCHF6 occurs due to reduced auto-ubiquitination, as this effect is blocked by inhibition
571 of the ER-associated degradation pathway or by mutation of residues essential for MARCHF6
572 activity. The precise mechanism by which low oxygen levels impede MARCHF6
573 auto-ubiquitination remains unclear, although the involvement of asparagine hydroxylation or
574 accumulated squalene was ruled out. We previously found that cholesterol and several of its
575 biosynthetic intermediates, including lanosterol, also impede MARCHF6 degradation [37].
576 This raises the possibility that a lanosterol-dependent mechanism promotes MARCHF6
577 accumulation during hypoxia, which is particularly intriguing given that MARCHF6 also
578 targets lanosterol demethylase for degradation [62] and likely contributes to lanosterol

579 accumulation. It remains to be determined how increased MARCHF6 levels influence the
580 activity of its other metabolic substrates. These include the lipid droplet biogenesis protein
581 perilipin-2 [63] and the thyroid hormone-activating deiodinase DIO2 [64], which both function
582 in pathways perturbed by hypoxia [48, 65]. Unexpectedly, MARCHF6 levels were slightly but
583 significantly reduced upon treatment with exogenous squalene. This was also observed for the
584 saturated analogue squalane, and therefore is not a squalene-specific effect. Rather, it may
585 suggest that the stability of the 14-transmembrane domain MARCHF6 protein is sensitive to
586 membrane perturbations resulting from the delivery of large amounts of exogenous lipid.

587 A key finding of this study is that upon the hypoxia-induced delivery of SM to the
588 proteasome, accumulated squalene inhibits its complete degradation and liberates the
589 constitutively active trunSM. This feedforward mechanism, by which the substrate of SM
590 preserves its activity, is mediated by the SM-N100 regulatory domain and functional under
591 normoxic conditions. Here, it likely buffers against transient increases in squalene levels.
592 Accumulation of trunSM occurs even when MARCHF6 is depleted, indicating that squalene
593 similarly prevents the complete degradation of SM molecules targeted to the proteasome by
594 other E3 ubiquitin ligases. These additional regulators, and the factors controlling their
595 ubiquitination of SM, await future discovery and may shed light on how the SM-N100
596 regulatory domain undergoes MARCHF6-independent proteasomal degradation during
597 hypoxia. Although hypoxia and lipid accumulation can trigger ER stress and altered
598 proteostasis [66], the ability of squalene and farnesyl-containing compounds to allosterically
599 bind the SM-N100 domain [8] strongly indicates that squalene induces SM truncation directly,
600 rather than *via* bulk membrane effects. The specificity of this response is further supported by
601 the inability of its saturated analog squalane to induce truncation. While squalene is the most
602 likely of the farnesyl-containing cholesterol synthesis intermediates to accumulate under
603 normal conditions, owing to the rate-limiting and oxygen-dependent nature of SM activity, our
604 current and previous [8] data suggest that a farnesyl group alone is sufficient to promote
605 truncation. Precisely how this lipophilic moiety interferes with SM degradation is unknown,
606 although interaction with the membrane-embedded SM-N100 re-entrant loop [67] is a likely
607 possibility. SM also contains a short intrinsically disordered domain (residues 81–120) that is
608 required for its partial degradation and dictates the location of the truncation site [9], although
609 interaction of a farnesyl group with this region is more difficult to envision.

610 Previously, we reported that squalene and farnesyl-containing compounds also blunt
611 the MARCHF6-mediated ubiquitination of the SM-N100 domain, leading to stabilization of
612 full-length SM [8]. The existence of dual mechanisms enabling squalene to sustain SM activity
613 is intriguing, particularly as trunSM formation is itself dependent on ubiquitination [9]. One
614 possibility is that truncation is stimulated at a lower squalene threshold than the inhibition of
615 SM ubiquitination, allowing for a biphasic response to accumulating substrate. Another
616 possibility is that truncation is a 'failsafe' mechanism to preserve the activity of the SM
617 enzyme. This may be necessary when a reduced frequency of MARCHF6 ubiquitination is
618 insufficient to completely prevent targeting of SM to the proteasome. It may also apply in
619 situations where SM ubiquitination is promoted by other cellular stimuli. For instance, during

620 hypoxia, the stabilization of MARCHF6 may override the inhibitory effects of accumulated
621 squalene.

622 **Pathophysiological consequences of truncation**

623 Beyond hypoxia, our results point to additional contexts in which SM truncation has
624 physiological relevance. One of these is lipid droplets, which serve important functions in
625 triglyceride and cholesteryl ester storage as well as the sequestration of lipotoxic compounds,
626 including excess squalene [47, 68]. Lipid droplets can also serve as energy depots for fueling
627 cancer cell growth [69]. Although several proteomic studies have identified SM in lipid droplet
628 fractions [49–51], the detected peptides were unable to distinguish between its full-length and
629 truncated forms. Using immunofluorescence as well as immunoblotting, which remains the
630 most robust means of differentiating the two proteins, we found that only trunSM is capable of
631 localizing to lipid droplets. The absence of the membrane-embedded SM-N100 re-entrant loop,
632 which allows trunSM to adopt a peripheral ER membrane topology [9], also accounts for its
633 movement to the lipid droplet monolayer. By contrast, the C-terminal membrane-associated
634 helices of SM [44] appear to have a highly conserved role in lipid droplet localization, given
635 that they are also required for the partitioning of the yeast orthologue Erg1p [70, 71].

636 Further study is required to determine the functional consequences of lipid droplet-
637 localized trunSM. Curiously, the yeast orthologue of SM is inactive on lipid droplets due to the
638 absence of a microsomal electron donor [71]. Should this lack of activity hold for trunSM, lipid
639 droplets may nevertheless serve as a depot of stable enzyme that is inaccessible to polytopic
640 ER-associated degradation cofactors such as MARCHF6 [38], yet able to return to the ER *via*
641 contact sites [72, 73]. It is interesting to note that several other cholesterol synthesis enzymes
642 also partition to lipid droplets, most notably lanosterol synthase, the enzyme immediately
643 downstream of SM [49–51]. The yeast orthologue of this protein remains active on lipid
644 droplets [74], but whether this holds true in mammalian cells is unknown. The shuttling of
645 cholesterol synthesis intermediates such as squalene and lanosterol between the ER and lipid
646 droplets is an unexplored area with the potential for major consequences in the metabolic
647 feedback regulation of the pathway.

648 Both hypoxia and squalene accumulation trigger lipid droplet formation [48, 75], and
649 it is likely that these two phenomena are linked. As SM truncation occurs in the ER, the amount
650 of trunSM produced under squalene-rich conditions may be coupled with the ability of a cell
651 to adequately sequester this intermediate to lipid droplets. In cells with a low capacity for lipid
652 droplet biogenesis, rapid accumulation of squalene in the ER is expected to induce SM
653 truncation and facilitate its clearance. In cells with a greater capacity for lipid droplet
654 biogenesis, accumulation of squalene in the ER is likely to be less dramatic, resulting in a lower
655 level of truncation that is sufficient to clear this smaller quantity. Supporting this idea, a high
656 rate of lipid droplet biogenesis confers resistance to the toxic effects of SM inhibition in
657 neuroendocrine cancer cell lines [47].

658 Overexpression and overactivity of SM occurs in a wide range of malignancies
659 including hepatocellular carcinoma and prostate cancer, where it is positively correlated with

660 severity and lethality [21, 53]. Despite this, a specific examination of trunSM levels had not
661 been performed in any cancer type prior to our study. We found that total SM levels were
662 reduced in endometrial tumor tissues, which was unexpected given that high *SQLE* mRNA
663 expression is a risk factor for progression of this cancer [76]. However, the reduction in total
664 SM was accompanied by a marked increase in the proportion of the stable and constitutively
665 active trunSM. This was also well-correlated with the levels of HIF1α, suggesting that hypoxia-
666 induced truncation of SM occurs *in vivo*. An increased proportion of trunSM was observed in
667 endometrial tumors from both lean and obese patients, indicating that the phenomenon is likely
668 not influenced by obesity or circulating lipid levels. Our data indicate that trunSM may be a
669 contributing factor to cell growth and survival in the hypoxic tumor microenvironment, which
670 is noteworthy given that severe hypoxia is often associated with a poorer cancer prognosis [22].
671 It would be worthwhile for future studies to quantify the truncation of SM in cancer types
672 where its elevated protein expression has previously been identified, as well as in those that
673 show a particular propensity for hypoxia, such as prostate and pancreatic cancer [28]. Although
674 trunSM retains full catalytic activity and can likely fulfil the cholesterol synthesis-dependent
675 roles of SM in oncogenesis, further work is needed to confirm that it can enable the suite of
676 other oncogenic functions previously reported for full-length SM. To date, these include the
677 activation of ERK signaling [18] as well as interactions with carbonic anhydrase 3 [20], GSK3β
678 and p53 [19]. These cholesterol-independent effects of SM are likely to be most important
679 during severe hypoxia, where cholesterol synthesis cannot proceed.

680 Finally, although this study was largely performed using the extremely low oxygen
681 levels characteristic of pathophysiological hypoxia, we observed that SM truncation was
682 responsive to a range of 'physoxic' oxygen levels that occur within normal tissues *in situ*. This
683 reinforces the concept of truncation as a buffering mechanism to accommodate normal
684 substrate fluctuations, which may be important for preventing squalene-induced dysfunction in
685 tissues with lower oxygen perfusion, such as the brain [28]. Squalene fluctuations also occur
686 diurnally [77] and with changing sterol status [4], and its levels can vary dramatically between
687 different tissues [78]. Thus, the ability of squalene to stimulate formation of the rate-limiting
688 trunSM may play an important role in regulating flux through cholesterol synthesis under
689 varying physiological conditions.

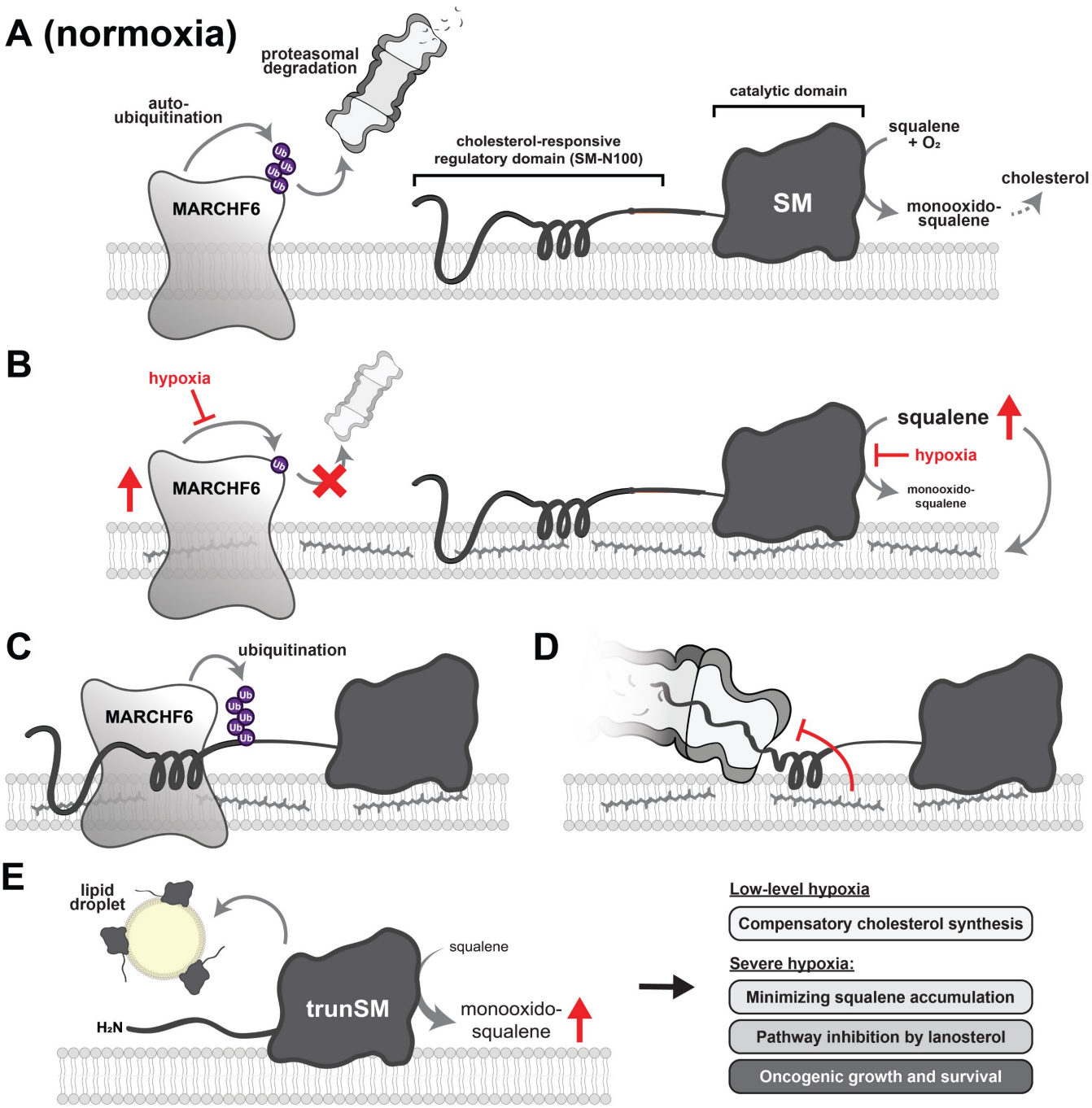

Figure 7. Model of hypoxia-induced SM truncation.

(A, B) Hypoxic conditions inhibit the auto-ubiquitination of the E3 ubiquitin ligase MARCHF6, resulting in its stabilization. Simultaneously, the SM-catalyzed conversion of squalene to monooxidosqualene is inhibited, leading to squalene accumulation. **(C)** Increased MARCHF6 activity promotes the targeting of SM to the proteasome. **(D)** Squalene binds the SM-N100 domain and impedes the complete proteasomal degradation of SM, leading to **(E)** the formation of the constitutively active trunSM, which is capable of localizing to lipid droplets. During transient or low-level hypoxia, trunSM activity may facilitate continued cholesterol synthesis to compensate for the oxygen shortfall. During long-term or severe

700 hypoxia, trunSM activity may reduce squalene-induced toxicity while also promoting the
701 formation of lanosterol, which suppresses an early step of the cholesterol synthesis pathway.
702 During pathophysiological hypoxia, trunSM may enable continued cell growth and survival
703 *via* both cholesterol synthesis-dependent and -independent oncogenic properties.

704 # Materials and methods

705 ## Reagents and cell lines

706 Fetal calf serum (FCS), newborn calf serum (NCS), high-glucose Dulbecco's Modified
707 Eagle's Medium (DMEM-HG), penicillin/streptomycin, Opti-MEM reduced serum medium,
708 RNAiMAX transfection reagent, Lipofectamine 3000 transfection reagent, TRI reagent, the
709 SuperScript III First-Strand Synthesis kit, the PureLink Genomic DNA Mini kit, HCS
710 LipidTOX Deep Red Neutral Lipid Stain, and BODIPY 493/503 were from Thermo Fisher
711 (Carlsbad, CA, USA). Lipoprotein-deficient serum (LPDS, 30 mg/mL protein) was prepared
712 from FCS by density gradient centrifugation and dialysis, as described in [79]. Primers, small
713 interfering RNA (siRNA), protease inhibitor cocktail, and Tween-20 were from Sigma-Aldrich
714 (St Louis, MO, USA). Tris-glycine SDS-PAGE gels were prepared in-house. Immobilon
715 Western chemiluminescent HRP substrate and nitrocellulose membranes were from Millipore
716 (Burlington, MA, USA). The QuantiNova SYBR Green PCR kit was from Qiagen (Hilden,
717 GE). Skim milk powder was from Fonterra (Richmond, VIC, AU). The Lipid Droplet Isolation
718 Kit was from Cell Biolabs Inc. (San Diego, CA, USA). Chemicals were from the following
719 suppliers: 2,3,22,23-dioxidosqualene (Echelon Biosciences S-0302), 2,3-oxidosqualene
720 (monooxidosqualene; Echelon Biosciences S-0301), 5α-cholestane (Sigma-Aldrich C8003),
721 bafilomycin A1 (Sigma-Aldrich B1793), BIBB 515 (Cayman Chemical 10010517), CB-5083
722 (Cayman Chemical 16276), DM-NOFD (Sigma-Aldrich SML1874), DMOG (Sigma-Aldrich
723 D3695), FG-4592 (Cayman Chemical 15294), GR70585X (GlaxoSmithKlein),
724 mevalonolactone (Sigma-Aldrich M4667), mevastatin (Sigma-Aldrich M2537), MG132
725 (Sigma-Aldrich C2211), NB-598 (Chemscene CS-1274), oleate-bovine serum albumin
726 complexes (Sigma-Aldrich O3008), squalane (Sigma-Aldrich 234311), squalene (Sigma-
727 Aldrich S3626), TAK-475 (Sigma-Aldrich SML2168).

728 HEK293T cells were a gift from the UNSW School of Medical Sciences (UNSW
729 Sydney, NSW, Australia), HCT116 cells were a gift from Dr Ewa Goldys (UNSW Sydney,
730 NSW, Australia), Huh7 cells were a gift from the Centre for Cardiovascular Research (UNSW
731 Sydney NSW, Australia), MBA-MB-231 and HeLaT cells were gifts from Dr Louise Lutze-
732 Mann and Dr Noel Whitaker (UNSW Sydney, NSW, Australia), and HeLa cells were obtained
733 from the American Type Culture Collection. HEK293 cells stably expressing
734 SM-N100-GFP-V5, MARCHF6-V5, MARCHF6-V5 C9A, or MARCHF6-V5 N890A were
735 generated previously using the Flp-In T-Rex system [36, 37].

736 ## Cell culture

737 Cells were maintained in a humidified Heraeus BB 15 incubator at 37 °C, 5% CO_2, and
738 21% O_2 (normoxia) in maintenance medium (DMEM-HG, 10% [v/v] FCS, 100 U/mL
739 penicillin, 100 μg/mL streptomycin). To improve HEK293 and HEK293T cell surface
740 adhesion, culture vessels were treated with 25 μg/mL polyethyleneimine in phosphate-buffered
741 saline (PBS) for 15 min at 37 °C prior to cell seeding. Plasmid and siRNA transfections were
742 performed in maintenance medium lacking penicillin and streptomycin. Sterol depletions were

743 performed in maintenance medium containing LPDS. Hypoxic incubations at 0.5–10% O_2
744 were performed in a humidified Binder CB 150 incubator at 37 °C and 5% CO_2. For all
745 treatments, appropriate solvent controls were used (water [DMOG]; ethanol (mevalonolactone,
746 GR70585X); dimethyl sulfoxide [CB-5083, MG132, bafilomycin A1, DM-NOFD, mevastatin,
747 TAK-475, BIBB-515, NB-598]; dimethyl sulfoxide containing 1% [v/v] Tween-20 [squalene,
748 monooxidosqualene, dioxidosqualene, squalane]) and the final concentration of solvent did not
749 exceed 1% (v/v) in cell culture medium. Treatments were delivered in full medium refreshes,
750 and all experiments were 48–72 h in duration.

751 **Plasmids**

752 Plasmids encoding Cas9 and *SQLE*-targeting guide RNAs were generated by *BbsI*
753 cloning into a PX458 vector as described in [80]. Amino acid substitutions (SM Y195F) within
754 expression vectors were generated using the overlap extension cloning method, as described
755 previously [81]. The identity of all plasmids was confirmed *via* Sanger dideoxy sequencing.
756 The plasmids used in this study are listed in Supplementary Table 1, and the primer sequences
757 used for DNA cloning are listed in Supplementary Table 2.

758 **siRNA and plasmid transfection**

759 To downregulate gene expression or transiently overexpress proteins, cells were seeded
760 into 12-well plates. The next day, cells were transfected with 15 pmol siRNA using RNAiMAX
761 (Invitrogen; 15 pmol siRNA : 2 µL reagent) or 1 µg expression vector using Lipofectamine
762 3000 (Invitrogen; 1 µg DNA : 2 µL reagent with 2 µL P3000 supplemental reagent), delivered
763 in Opti-MEM. After 24 h, cells were refreshed in maintenance medium and treated as specified
764 in figure legends. The siRNAs and plasmids used in this study are listed in Supplementary
765 Table 1.

766 **Protein harvest and immunoblotting**

767 To quantify protein levels, cells were seeded into 6- or 12-well plates and treated as
768 specified in figure legends. For detection of SM, total protein was harvested in 2% SDS lysis
769 buffer (10 mM Tris-HCl [pH 7.6], 2% [w/v] SDS, 100 mM NaCl, 2% [v/v] protease inhibitor
770 cocktail), passed through a 21-gauge needle until homogenous, and vortexed at room
771 temperature for 20 min. For detection of MARCHF6, cells were scraped in ice-cold PBS,
772 pelleted, and lysed in modified RIPA buffer (50 mM Tris-HCl [pH 8.0], 0.1% [w/v] SDS,
773 1.5% [w/v] IGEPAL CA-630, 0.5% [w/v] sodium deoxycholate, 150 mM NaCl, 2 mM $MgCl_2$,
774 2% [v/v] protease inhibitor cocktail), passed 20 times through a 22-gauge needle, rotated at
775 4 °C for 30 min, and centrifuged at 17,000 *g* and 4 °C for 15 min to obtain the supernatant.
776 Lysate protein content was quantified using the bicinchoninic acid assay (Thermo Fisher), and
777 sample concentrations were normalized by dilution in the appropriate lysis buffer and 0.25 vol
778 5× Laemmli buffer (250 mM Tris-HCl [pH 6.8], 10% [w/v] SDS, 25% [v/v] glycerol,

779 0.2% [w/v] bromophenol blue, 5% [v/v] β-mercaptoethanol). For SM detection, normalized
780 samples were heated at 95°C for 5 min.

781 Proteins were separated by 10% (w/v) Tris-glycine SDS-PAGE, electroblotted onto
782 nitrocellulose membranes, and blocked in 5% (w/v) skim milk powder in PBS containing
783 0.1% (v/v) Tween-20 (PBST). Immunoblotting was performed using the following antibodies:
784 rabbit polyclonal anti-HIF1α (Proteintech 20960-1-AP; 1:1,000 at room temperature for 1 h),
785 rabbit polyclonal anti-SM(SQLE) (Proteintech 12544-1-AP; 1:2,500 at 4 °C for 16 h), rabbit
786 monoclonal anti-GAPDH (Cell Signaling Technology 2118; 1:2,000 at 4 °C for 16 h), mouse
787 monoclonal anti-V5 (Thermo Fisher R960-25; 1:5,000 at room temperature for 1 h), rabbit
788 monoclonal anti-HA (Cell Signaling Technology 3724; 1:2,000 at 4 °C for 16 h), rabbit
789 monoclonal anti-calnexin (Cell Signaling Technology 2679; 1:1,000 at 4 °C for 16 h), rabbit
790 polyclonal anti-ABHD5 (Proteintech 12201-1-AP; 1:1,000 at 4 °C for 16 h), mouse
791 monoclonal anti-pan-14-3-3 (Santa Cruz Biotechnology sc-1657 ; 1:1,000 at 4 °C for 16 h),
792 IRDye 680RD donkey anti-rabbit IgG (LI-COR Biosciences LCR-926-68073; 1:5,000), IRDye
793 800CW donkey anti-mouse IgG (LI-COR Biosciences LCR-926-32212; 1:10,000 at room
794 temperature for 1 h), peroxidase-conjugated AffiniPure donkey anti-rabbit IgG (Jackson
795 ImmunoResearch Laboratories 711-035-152; 1:10,000 at room temperature for 1 h), and
796 peroxidase-conjugated AffiniPure donkey anti-mouse IgG (Jackson ImmunoResearch
797 Laboratories 715-035-150; 1:10,000 at room temperature for 1 h). All antibodies were diluted
798 in 5% (w/v) bovine serum albumin in PBST containing 0.02% (w/v) sodium azide, except for
799 anti-HIF1α and peroxidase-conjugated antibodies, which were diluted in 5% (w/v) skim milk
800 powder in PBST. Fluorescence-based detection of SM and trunSM, GAPDH, and $(HA)_3$-
801 SM-V5 was performed using an Odyssey CLx imager (LI-COR Biosciences), and enhanced
802 chemiluminescence-based detection of HIF1α, MARCHF6-V5, SM and trunSM (fractionated
803 and tissue-derived lysates), calnexin, ABHD5, GAPDH (fractionated lysates) and 14-3-3 was
804 performed using Immobilon Western chemiluminescent HRP substrate (Millipore) and an
805 ImageQuant LAS 500 imager (Cytiva Life Sciences). Densitometry analysis was performed
806 using Image Studio Lite v5.2.5 (LI-COR Biosciences).

807 **RNA harvest and qRT-PCR**

808 To quantify gene expression, cells were seeded into 12-well plates and treated as
809 specified in figure legends. Total RNA was harvested using TRI reagent (Sigma-Aldrich) and
810 polyadenylated RNA was reverse transcribed using the SuperScript III First Strand Synthesis
811 kit (Invitrogen). cDNA products were used as the template for quantitative reverse
812 transcription-PCR (qRT-PCR) in technical triplicate using the QuantiNova SYBR Green PCR
813 kit (Qiagen). mRNA levels were normalized to the geometric mean of *RPL11*, *GAPDH* and
814 *ACTB* for hypoxia experiments, or *PBGD* for validation of siRNA knockdowns and gene
815 knockout, using the comparative C_T method [82]. Normalized data were adjusted relative to
816 the control condition, as specified in figure legends. The primer sequences used for qRT-PCR
817 in this study are listed in Supplementary Table 2.

818 **Gas chromatography-mass spectrometry**

819 To quantify cellular squalene levels, gas chromatography-mass spectrometry was
820 performed as described previously [8]. Briefly, cells in 6-well plates were lysed in 0.05 M
821 NaOH, total protein was quantified using the bicinchoninic acid assay, and samples were
822 adjusted to the lowest protein concentration using 0.05 M NaOH plus 4 µg 5α-cholestane as an
823 internal standard, in a total volume of 1 mL. Lysates were mixed with 1 mL 100% (v/v)
824 ethanol, 500 µL 75% (w/v) KOH, 1 µL 20 mM butylated hydroxytoluene, and 20 µL 20 mM
825 EDTA, and saponified at 70 °C for 1 h. Non-saponifiable lipids were extracted by mixing with
826 1 mL 100% (v/v) ethanol and 2.5 mL hexane, centrifuging at 4,000 *g* for 5 min, and collection
827 of 2 mL of the organic phase. Lipids were dried in a vacuum centrifuge, resuspended in 50 µL
828 *N*,*O*-bis(trimethylsilyl)trifluoroacetamide, and derivatized at 60 °C for 1 h.

829 Derivatized lipids (1.5 µL) were injected *via* a heated (300 °C) splitless with surge
830 (38.0 psi for 0.50 min) inlet into a Thermo Trace gas chromatograph fitted with a Trace
831 TR-50MS GC column (60 m × 0.25 mm, 0.25 µm film thickness, Thermo Fisher). Analytes
832 were separated with helium as the carrier gas at a constant flow of 1.2 ml/min with vacuum
833 compensation, and temperature programming as follows: 70 °C for 0.70 min, 20 °C/min to
834 250 °C, 3 °C/min to 270 °C, 1.5 °C/min to 315 °C, then hold for 10 min. The GC column was
835 coupled to a Thermo DSQIII mass spectrometer, with a transfer line temperature of 320 °C and
836 an ion source temperature of 250 °C. For mass spectrometry analysis, the electron energy was
837 70 eV, the emission current was 130 µA and the detector gain was 3.0×10^5. Squalene and
838 5α-cholestane standards were analyzed in scan mode (34–600 Da) to identify peaks and
839 retention times, and identity was confirmed using the National Institute of Standards and
840 Technology databases. Experimental samples were analyzed in selective ion monitoring mode
841 to detect squalene (m/z = 81.0, 410.4) and 5α-cholestane (m/z = 149.1, 217.2, 372.4), with a
842 detection width of 0.1 and dwell time of 200 ms. Chromatograph peaks were integrated using
843 Thermo Xcalibur software (v2.2 SP1.48) and the peak area of squalene was normalized to the
844 5α-cholestane internal standard. A squalene standard curve ranging from 3.125–100 ng/µL was
845 used to quantify squalene levels, with data adjusted to the total protein content of the cell lysate.

846 **Generation of SM knockout cells**

847 To knock out SM using CRISPR/Cas9, guide RNAs targeting the *SQLE* proximal
848 promoter (hg38 chr8:124998048–124998067; AATGGAAACGTTCCGACCCG) and first
849 exon (hg38 chr8:124999588–124999607; ATCCGAGAAGAGGGCGAACT) were designed
850 using CHOPCHOP [83] and cloned into the Cas9- and GFP-encoding PX598 vector using BbsI
851 restriction enzyme cloning, as described in [80]. HEK293T cells were seeded into 10 cm dishes
852 and transfected with 5 µg of both vectors using Lipofectamine 3000, as described above. After
853 24 h, cells were trypsinized, washed with PBS and resuspended in FACS buffer (5% [v/v] FCS
854 and 10 mM EDTA in PBS). Cells were sorted based on GFP fluorescence using a
855 BD FACSAria III at the UNSW Flow Cytometry Facility. GFP-positive cells were seeded into
856 10 cm dishes at a low density (6,000–12,000 cells/dish) and allowed to adhere for 2–3 weeks.
857 Single colonies were picked, expanded, and screened for *SQLE* mRNA expression and SM

858 protein expression *via* qRT-PCR and immunoblotting, as described above. To confirm the
859 genomic lesion, genomic DNA was isolated from clones using the PureLink Genomic DNA
860 Mini kit (Thermo Fisher). The CRISPR/Cas9 target region was amplified and cloned into a
861 pcDNA3.1 vector for Sanger dideoxy sequencing. The primer sequences used for guide RNA
862 generation are listed in Supplementary Table 2.

863 **Immunofluorescence and lipid droplet staining**

864 To detect protein lipid droplet localization, cells were seeded onto coverslips in
865 6-well plates and treated as specified in figure legends. Cells were fixed with 4% (w/v)
866 paraformaldehyde for 15 min, permeabilized in 0.1% (w/v) Triton X-100 for 10 min and
867 blocked in 3% (w/v) bovine serum albumin in PBS for 1 h at room temperature. If required,
868 coverslips were incubated in anti-HA (Cell Signaling Technology 3724; 1:100) or anti-V5
869 (Thermo Fisher R960-25; 1:500) antibody diluted in blocking solution for 16 h at 4 °C,
870 followed by incubation in goat anti-rabbit Alexa Fluor 568 (Thermo Fisher A-11011; 1:1,000)
871 or goat anti-mouse Alexa Fluor 568 (Thermo Fisher A-11004; 1:1,000) in blocking solution
872 for 1 h at room temperature. To stain lipid droplets, coverslips were incubated in 1 µg/mL
873 BODIPY 493/503 in PBS for 10 min at room temperature, or HCS LipidTOX Deep Red
874 Neutral Lipid Stain (1:500 in PBS) for 1 h. Coverslips were mounted in ProLong Gold Antifade
875 Mountant with DAPI and confocal microscopy was performed using a Zeiss LSM 900 confocal
876 microscope system equipped with a 63×/1.4 oil objective (Zeiss, Jena, Germany). The
877 fluorochromes used were Alexa Fluor 488 (GFP, BODIPY 493/503), Alexa Fluor 568 (V5-
878 and HA-tagged proteins), Cy5 (LipidTOX Deep Red) and DAPI. Images were inspected using
879 Fiji software and lipid droplet association was quantified as the percentage of transfected cells
880 showing lipid droplet-proximal localization of the protein or epitope of interest.

881 **Lipid droplet fractionation**

882 To isolate lipid droplets, cells were seeded into 10 cm dishes and treated as specified in
883 figure legends. Cell lysates were collected, a small aliquot was taken for total protein analysis,
884 and the remainder was fractionated using the Lipid Droplet Isolation Kit (Cell Biolabs Inc.).
885 The floating lipid droplet fraction and an intermediate cytosolic fraction were collected, while
886 the pellet was resuspended in 2% SDS lysis buffer and passed through a 21-gauge needle until
887 homogenous. Total protein within each fraction was quantified using the bicinchoninic acid
888 assay and equal amounts were subjected to immunoblotting. Lipid droplet partitioning was
889 expressed as the ratio between protein levels in the lipid droplet and pellet fractions, and
890 normalized to that of the lipid droplet marker ABHD5.

891 **Endometrial cancer tissues**

892 Matched tumor and adjacent benign endometrial tissues were obtained from lean (body
893 mass index <27 kg/m^2; n = 7) and obese (body mass index >30 kg/m^2; n = 7) postmenopausal
894 endometrioid adenocarcinoma patients recruited at the Royal Hospital for Women and Prince

895 of Wales Private Hospital (Randwick, Sydney, Australia), as described in [84]. Consent was
896 received from all patients prior to sample collection, and all processing and experiments were
897 approved by the Human Research Ethics Committee (HREC) of the South Eastern Sydney
898 Local Health District (HREC 15/339). Protein was isolated from powdered tissues using the
899 AllPrep DNA/RNA/Protein Mini Kit (Qiagen). Protein pellets were lysed in HES-SDS buffer
900 (20 mM HEPES [pH 7.4], 2% [w/v] SDS, 250 mM sucrose, 1 mM EDTA) and mixed with
901 1 vol 10% (w/v) SDS. Samples were homogenized using a handheld homogenizer and
902 centrifuged at 15,000 *g* for 5 min. The protein content of the clarified supernatant was
903 quantified using the bicinchoninic acid assay. Samples were diluted in 0.25 vol 5× Laemmli
904 buffer and heated at 65 °C for 5 min prior to SDS-PAGE and immunoblotting.

905 **Data analysis and presentation**

906 Data were normalized as described in figure legends. All data were obtained from $n \geq 2$
907 independent experiments, and visualization and statistical testing were performed using
908 GraphPad Prism v9.0 (GraphPad Software Inc.) as specified in figure legends. Where multiple
909 statistical tests were conducted within a single experiment, *p*-values were corrected using the
910 Benjamini-Hochberg method [85] with a false discovery threshold of 5%. Thresholds for
911 statistical significance were defined as: *, $p \leq 0.05$; **, $p \leq 0.01$. Values of $0.05 < p < 0.075$
912 are indicated in text on graphs. Figures were assembled using Adobe Illustrator v26.3 (Adobe
913 Inc.).

914 Acknowledgements

915 We thank Isabelle Capell-Hattam for assistance with CRISPR/Cas9, Dr Martin
916 Bucknall for technical assistance with GC/MS, and the members of the Brown laboratory for
917 critically reviewing this manuscript. We are also grateful to the patients from whom tissue
918 samples were collected, and staff at the Royal Hospital for Women and Prince of Wales Private
919 Hospital (Randwick, NSW, Australia) who assisted with surgical procedures. H.W.C. is
920 supported by an Australian Research Training Program scholarship, R.F. is supported by a
921 RANZCOG Mary Elizabeth Courier Research Scholarship, F.L.B. is supported by a Cancer
922 Institute NSW Career Development Fellowship (2021/CDF1120), and the Brown laboratory is
923 supported by Australian Research Council Grant DP170101178 and an NSW Health
924 Investigator Development Grant.

925 Author contributions

926 H.W.C.: conceptualization, methodology, investigation, visualization, writing –
927 original draft. E.M.O.: investigation. X.D.: methodology, investigation, visualization. R.F.:
928 resources, funding acquisition. H.Y.: resources, funding acquisition. F.L.B.: resources, writing

– review and editing, funding acquisition. A.J.B.: conceptualization, methodology, resources, writing – review and editing, supervision, funding acquisition.

Competing interests

The authors declare that there are no competing interests associated with the manuscript.

References

1. Baigent, C., Blackwell, L., Emberson, J., Holland, L. E., Reith, C., Bhala, N., Peto, R., Barnes, E. H., Keech, A., Simes, J., Collins, R., De Lemos, J., Braunwald, E., Blazing, M., Murphy, S., Downs, J. R., Gotto, A., Clearfield, M., Holdaas, H., Gordon, D., Davis, B., Koren, M., Dahlof, B., Poulter, N., Sever, P., Knopp, R. H., Fellström, B., Jardine, A., Schmieder, R., Zannad, F., Goldbourt, U., Kaplinsky, E., Colhoun, H. M., Betteridge, D. J., Durrington, P. N., Hitman, G. A., Fuller, J., Neil, A., Wanner, C., Krane, V., Sacks, F., Moyé, L., Pfeffer, M., Hawkins, C. M., Barter, P., Tavazzi, L., Maggioni, A., Marchioli, R., Tognoni, G., Franzosi, M. G., Bloomfield, H., Robins, S., Armitage, J., Parish, S., Sleight, P., Pedersen, T. R., Ridker, P. M., Holman, R., Meade, T., MacMahon, S., Marschner, I., Tonkin, A., Shaw, J., Serruys, P. W., Nakamura, H., Knatterud, G., Furberg, C., Byington, R., Macfarlane, P., Cobbe, S., Ford, I., Murphy, M., Blauw, G. J., Packard, C., Shepherd, J., Kjekshus, J., Wilhelmsen, L., Cannon, C., Bowman, L., Baxter, A., Landray, M., La Rosa, J., Rossouw, J., Probstfield, J., Flather, M., Kastelein, J., Newman, C., Shear, C., Tobert, J., Varigos, J., White, H., Yusuf, S., Mellies, M., McGovern, M., Barclay, J., Belder, R., Mitchel, Y., Musliner, T., Ansquer, J. C., Llewellyn, M., Bortolini, M., Brandrup-Wognsen, G., Bryzinski, B., Olsson, G., Pears, J., De Micco, D., Buck, G., Herrington, W. G., Kearney, P. M., Kirby, A., Lewis, D. A., Pollicino, C., and Sourjina, T. (2010) Efficacy and safety of more intensive lowering of LDL cholesterol: a meta-analysis of data from 170 000 participants in 26 randomised trials. *Lancet*. **376**, 1670–1681

2. Brown, A. J., Coates, H. W., and Sharpe, L. J. (2021) Cholesterol synthesis. in *Biochemistry of Lipids, Lipoproteins and Membranes*, 7th Ed. (Ridgway, N. D., and McLeod, R. S. eds), pp. 317–355, Elsevier Science

3. Porter, F. D., and Herman, G. E. (2011) Malformation syndromes caused by disorders of cholesterol synthesis. *J. Lipid Res.* **52**, 6–34

4. Gill, S., Stevenson, J., Kristiana, I., and Brown, A. J. (2011) Cholesterol-dependent degradation of squalene monooxygenase, a control point in cholesterol synthesis beyond HMG-CoA reductase. *Cell Metab.* **13**, 260–273

5. Bai, M., Xiao, X., and Prestwich, G. (1992) Epoxidation of 2,3-oxidosqualene to 2,3;22,23-squalene dioxide by squalene epoxidase. *Biochem. Biophys. Res. Commun.* **185**, 323–329

6. Horton, J. D., Shah, N. A., Warrington, J. A., Anderson, N. N., Park, S. W., Brown, M. S., and Goldstein, J. L. (2003) Combined analysis of oligonucleotide microarray data

968 from transgenic and knockout mice identifies direct SREBP target genes. *Proc. Natl.*
969 *Acad. Sci.* **100**, 12027–12032

970 7. Chua, N. K., Howe, V., Jatana, N., Thukral, L., and Brown, A. J. (2017) A conserved
971 degron containing an amphipathic helix regulates the cholesterol-mediated turnover of
972 human squalene monooxygenase, a rate-limiting enzyme in cholesterol synthesis. *J.*
973 *Biol. Chem.* **292**, 19959–19973

974 8. Yoshioka, H., Coates, H. W., Chua, N. K., Hashimoto, Y., Brown, A. J., and Ohgane,
975 K. (2020) A key mammalian cholesterol synthesis enzyme, squalene monooxygenase,
976 is allosterically stabilized by its substrate. *Proc. Natl. Acad. Sci.* **117**, 7150–7158

977 9. Coates, H. W., Capell-Hattam, I. M., and Brown, A. J. (2021) The mammalian
978 cholesterol synthesis enzyme squalene monooxygenase is proteasomally truncated to a
979 constitutively active form. *J. Biol. Chem.* **296**, 100731

980 10. Kuzu, O. F., Noory, M. A., and Robertson, G. P. (2016) The role of cholesterol in cancer.
981 *Cancer Res.* **76**, 2063–2070

982 11. Brown, D. N., Caffa, I., Cirmena, G., Piras, D., Garuti, A., Gallo, M., Alberti, S.,
983 Nencioni, A., Ballestrero, A., and Zoppoli, G. (2016) Squalene epoxidase is a bona fide
984 oncogene by amplification with clinical relevance in breast cancer. *Sci. Rep.* **6**, 19435

985 12. Stopsack, K. H., Gerke, T. A., Sinnott, J. A., Penney, K. L., Tyekucheva, S., Sesso, H.
986 D., Andersson, S.-O. O., Cerhan, R., Giovannucci, E. L., Mucci, L. A., Rider, J. R.,
987 Andrén, O., Cerhan, J. R., Giovannucci, E. L., Mucci, L. A., and Rider, J. R. (2016)
988 Cholesterol metabolism and prostate cancer lethality. *Cancer Res.* **76**, 4785–4790

989 13. Pudova, E. A., Krasnov, G. S., Kobelyatskaya, A. A., Savvateeva, M. V., Fedorova, M.
990 S., Pavlov, V. S., Nyushko, K. M., Kaprin, A. D., Alekseev, B. Y., Trofimov, D. Y.,
991 Sukhikh, G. T., Snezhkina, A. V., and Kudryavtseva, A. V. (2021) Gene expression
992 changes and associated pathways involved in the progression of prostate cancer
993 advanced stages. *Front. Genet.* **11**, 613162

994 14. Bai, R., Rebelo, A., Kleeff, J., and Sunami, Y. (2021) Identification of prognostic lipid
995 droplet-associated genes in pancreatic cancer patients via bioinformatics analysis. *Lipids*
996 *Health Dis.* **20**, 58

997 15. Parris, T. Z., Kovacs, A., Hajizadeh, S., Nemes, S., Semaan, M., Levin, M., Karlsson,
998 P., and Helou, K. (2014) Frequent MYC coamplification and DNA hypomethylation of
999 multiple genes on 8q in 8p11-p12-amplified breast carcinomas. *Oncogenesis*. **3**, e95

1000 16. Yang, F., Kou, J., Liu, Z., Li, W., and Du, W. (2021) MYC enhances cholesterol
1001 biosynthesis and supports cell proliferation through SQLE. *Front. Cell Dev. Biol.* **9**,
1002 655889

1003 17. Sun, H., Li, L., Li, W., Yang, F., Zhang, Z., Liu, Z., and Du, W. (2021) p53
1004 transcriptionally regulates SQLE to repress cholesterol synthesis and tumor growth.
1005 *EMBO Rep.* **22**, e52537

1006 18. He, L., Li, H., Pan, C., Hua, Y., Peng, J., Zhou, Z., Zhao, Y., and Lin, M. (2021)
1007 Squalene epoxidase promotes colorectal cancer cell proliferation through accumulating
1008 calcitriol and activating CYP24A1-mediated MAPK signaling. *Cancer Commun.* **41**,

1009 726–746

1010 19. Jun, S. Y., Brown, A. J., Chua, N. K., Yoon, J.-Y., Lee, J.-J., Yang, J. O., Jang, I., Jeon,
1011 S.-J., Choi, T.-I., Kim, C.-H., and Kim, N.-S. (2021) Reduction of squalene epoxidase
1012 by cholesterol accumulation accelerates colorectal cancer progression and metastasis.
1013 *Gastroenterology*. **160**, 1194-1207.e28

1014 20. Liu, D., Wong, C. C., Zhou, Y., Li, C., Chen, H., Ji, F., Go, M. Y. Y., Wang, F., Su, H.,
1015 Wei, H., Cai, Z., Wong, N., Wong, V. W. S., and Yu, J. (2021) Squalene epoxidase
1016 induces nonalcoholic steatohepatitis via binding to carbonic anhydrase 3 and is a
1017 therapeutic target. *Gastroenterology*. 10.1053/j.gastro.2021.02.051

1018 21. Liu, D., Wong, C. C., Fu, L., Chen, H., Zhao, L., Li, C., Zhou, Y., Zhang, Y., Xu, W.,
1019 Yang, Y., Wu, B., Cheng, G., Lai, P. B.-S., Wong, N., Sung, J. J., and Yu, J. (2018)
1020 Squalene epoxidase drives NAFLD-induced hepatocellular carcinoma and is a direct
1021 pharmaceutical target. *Sci. Transl. Med.* **10**, eaap9840

1022 22. Rankin, E. B., and Giaccia, A. J. (2016) Hypoxic control of metastasis. *Science*. **352**,
1023 175–180

1024 23. Haider, S., McIntyre, A., van Stiphout, R. G. P. M., Winchester, L. M., Wigfield, S.,
1025 Harris, A. L., and Buffa, F. M. (2016) Genomic alterations underlie a pan-cancer
1026 metabolic shift associated with tumour hypoxia. *Genome Biol.* **17**, 1–17

1027 24. Mukodani, J., Ishikawa, Y., and Fukuzaki, H. (1990) Effects of hypoxia on sterol
1028 synthesis, acyl-CoA:cholesterol acyltransferase activity, and efflux of cholesterol in
1029 cultured rabbit skin fibroblasts. *Arteriosclerosis*. **10**, 106–110

1030 25. Parathath, S., Mick, S. L., Feig, J. E., Joaquin, V., Grauer, L., Habiel, D. M., Gassmann,
1031 M., Gardner, L. B., and Fisher, E. A. (2011) Hypoxia is present in murine atherosclerotic
1032 plaques and has multiple adverse effects on macrophage lipid metabolism. *Circ. Res.*
1033 **109**, 1141–1152

1034 26. Wu, X., Niculite, C. M., Preda, M. B., Rossi, A., Tebaldi, T., Butoi, E., White, M. K.,
1035 Tudoran, O. M., Petrusca, D. N., Jannasch, A. S., Bone, W. P., Zong, X., Fang, F.,
1036 Burlacu, A., Paulsen, M. T., Hancock, B. A., Sandusky, G. E., Mitra, S., Fishel, M. L.,
1037 Buechlein, A., Ivan, C., Oikonomopoulos, S., Gorospe, M., Mosley, A., Radovich, M.,
1038 Davé, U. P., Ragoussis, J., Nephew, K. P., Mari, B., McIntyre, A., Konig, H., Ljungman,
1039 M., Cousminer, D. L., Macchi, P., and Ivan, M. (2020) Regulation of cellular sterol
1040 homeostasis by the oxygen responsive noncoding RNA lincNORS. *Nat. Commun.* **11**,
1041 4755

1042 27. Nguyen, A. D., McDonald, J. G., Bruick, R. K., and DeBose-Boyd, R. A. (2007)
1043 Hypoxia stimulates degradation of 3-hydroxy-3-methylglutaryl-coenzyme A reductase
1044 through accumulation of lanosterol and hypoxia-inducible factor-mediated induction of
1045 insigs. *J. Biol. Chem.* **282**, 27436–27446

1046 28. McKeown, S. R. (2014) Defining normoxia, physoxia and hypoxia in tumours-
1047 implications for treatment response. *Br. J. Radiol.* **87**, 20130676

1048 29. Dolt, K. S., Karar, J., Mishra, M. K., Salim, J., Kumar, R., Grover, S. K., and Qadar
1049 Pasha, M. A. (2007) Transcriptional downregulation of sterol metabolism genes in
1050 murine liver exposed to acute hypobaric hypoxia. *Biochem. Biophys. Res. Commun.* **354**,

1051 148–153

1052 30. Cao, R., Zhao, X., Li, S., Zhou, H., Chen, W., Ren, L., Zhou, X., Zhang, H., and Shi, R.
1053 (2014) Hypoxia induces dysregulation of lipid metabolism in HepG2 cells via activation
1054 of HIF-2α. *Cell. Physiol. Biochem.* **34**, 1427–1441

1055 31. Bellot, G., Garcia-Medina, R., Gounon, P., Chiche, J., Roux, D., Pouysségur, J., and
1056 Mazure, N. M. (2009) Hypoxia-induced autophagy is mediated through hypoxia-
1057 inducible factor induction of BNIP3 and BNIP3L via their BH3 domains. *Mol. Cell.*
1058 *Biol.* **29**, 2570–2581

1059 32. Hornbeck, P. V., Zhang, B., Murray, B., Kornhauser, J. M., Latham, V., and Skrzypek,
1060 E. (2015) PhosphoSitePlus, 2014: mutations, PTMs and recalibrations. *Nucleic Acids*
1061 *Res.* **43**, D512–D520

1062 33. Chua, N. K., Hart-Smith, G., and Brown, A. J. (2019) Non-canonical ubiquitination of
1063 the cholesterol-regulated degron of squalene monooxygenase. *J. Biol. Chem.* **294**, 8134–
1064 8147

1065 34. Ivan, M., Kondo, K., Yang, H., Kim, W., Valiando, J., Ohh, M., Salic, A., Asara, J. M.,
1066 Lane, W. S., and Kaelin, J. (2001) HIFα targeted for VHL-mediated destruction by
1067 proline hydroxylation: implications for O2 sensing. *Science*. **292**, 464–468

1068 35. Cockman, M. E., Lippl, K., Tian, Y. M., Pegg, H. B., Figg, W. D., Abboud, M. I., Heilig,
1069 R., Fischer, R., Myllyharju, J., Schofield, C. J., and Ratcliffe, P. J. (2019) Lack of
1070 activity of recombinant HIF prolyl hydroxylases (PHDs) on reported non-HIF
1071 substrates. *Elife*. 10.7554/ELIFE.46490

1072 36. Zelcer, N., Sharpe, L. J., Loregger, A., Kristiana, I., Cook, E. C., Phan, L., Stevenson,
1073 J., and Brown, A. J. (2014) The E3 ubiquitin ligase MARCH6 degrades squalene
1074 monooxygenase and affects 3-hydroxy-3-methyl-glutaryl coenzyme A reductase and the
1075 cholesterol synthesis pathway. *Mol. Cell. Biol.* **34**, 1262–1270

1076 37. Sharpe, L. J., Howe, V., Scott, N. A., Luu, W., Phan, L., Berk, J. M., Hochstrasser, M.,
1077 and Brown, A. J. (2019) Cholesterol increases protein levels of the E3 ligase MARCH6,
1078 and thereby stimulates protein degradation. *J. Biol. Chem.* **294**, 2436–2448

1079 38. Hassink, G., Kikkert, M., Voorden, S. Van, Lee, S.-J., Spaapen, R., Laar, T. Van,
1080 Coleman, C. S., Bartee, E., Uh, K. F., Chau, V., and Wiertz, E. (2005) TEB4 is a C4HC3
1081 RING finger-containing ubiquitin ligase of the endoplasmic reticulum. *Biochem. J.* **388**,
1082 647–655

1083 39. Zattas, D., Berk, J. M., Kreft, S. G., and Hochstrasser, M. (2016) A conserved C-terminal
1084 element in the yeast Doa10 and human MARCH6 ubiquitin ligases required for selective
1085 substrate degradation. *J. Biol. Chem.* **291**, 12105–12118

1086 40. Lando, D., Peet, D. J., Gorman, J. J., Whelan, D. A., Whitelaw, M. L., and Bruick, R.
1087 K. (2002) FIH-1 is an asparaginyl hydroxylase enzyme that regulates the transcriptional
1088 activity of hypoxia-inducible factor. *Genes Dev.* **16**, 1466–1471

1089 41. Scholz, C. C., Rodriguez, J., Pickel, C., Burr, S., Fabrizio, J. A., Nolan, K. A.,
1090 Spielmann, P., Cavadas, M. A. S., Crifo, B., Halligan, D. N., Nathan, J. A., Peet, D. J.,
1091 Wenger, R. H., Von Kriegsheim, A., Cummins, E. P., and Taylor, C. T. (2016) FIH

Regulates Cellular Metabolism through Hydroxylation of the Deubiquitinase OTUB1. *PLOS Biol.* **14**, e1002347

42. McDonough, M. A., McNeill, L. A., Tilliet, M., Papamicaël, C. A., Chen, Q. Y., Banerji, B., Hewitson, K. S., and Schofield, C. J. (2005) Selective inhibition of factor inhibiting hypoxia-inducible factor. *J. Am. Chem. Soc.* **127**, 7680–7681

43. Hauß, T., Dante, S., Dencher, N. A., and Haines, T. H. (2002) Squalane is in the midplane of the lipid bilayer: implications for its function as a proton permeability barrier. *Biochim. Biophys. Acta - Bioenerg.* **1556**, 149–154

44. Padyana, A. K., Gross, S., Jin, L., Cianchetta, G., Narayanaswamy, R., Wang, F., Wang, R., Fang, C., Lv, X., Biller, S. A., Dang, L., Mahoney, C. E., Nagaraja, N., Pirman, D., Sui, Z., Popovici-Muller, J., and Smolen, G. A. (2019) Structure and inhibition mechanism of the catalytic domain of human squalene epoxidase. *Nat. Commun.* **10**, 97

45. Chua, N. K., Coates, H. W., and Brown, A. J. (2020) Squalene monooxygenase: a journey to the heart of cholesterol synthesis. *Prog. Lipid Res.* **79**, 101033

46. Hong, Z., Liu, T., Wan, L., Fa, P., Kumar, P., Cao, Y., Prasad, C. B., Qiu, Z., Liu, J., Wang, H., Li, Z., Wang, Q.-E., Guo, P., Guo, D., Yilmaz, A. S., Lu, L., Papandreou, I., Jacob, N. K., Yan, C., Zhang, X., She, Q.-B., Ma, Z., and Zhang, J. (2022) Targeting squalene epoxidase interrupts homologous recombination via the ER stress response and promotes radiotherapy efficacy. *Cancer Res.* **82**, 1298–1312

47. Mahoney, C. E., Pirman, D., Chubukov, V., Sleger, T., Hayes, S., Fan, Z. P., Allen, E. L., Chen, Y., Huang, L., Liu, M., Zhang, Y., McDonald, G., Narayanaswamy, R., Choe, S., Chen, Y., Gross, S., Cianchetta, G., Padyana, A. K., Murray, S., Liu, W., Marks, K. M., Murtie, J., Dorsch, M., Jin, S., Nagaraja, N., Biller, S. A., Roddy, T., Popovici-Muller, J., and Smolen, G. A. (2019) A chemical biology screen identifies a vulnerability of neuroendocrine cancer cells to SQLE inhibition. *Nat. Commun.* **10**, 96

48. Bensaad, K., Favaro, E., Lewis, C. A., Peck, B., Lord, S., Collins, J. M., Pinnick, K. E., Wigfield, S., Buffa, F. M., Li, J. L., Zhang, Q., Wakelam, M. J. O., Karpe, F., Schulze, A., and Harris, A. L. (2014) Fatty acid uptake and lipid storage induced by HIF-1α contribute to cell growth and survival after hypoxia-reoxygenation. *Cell Rep.* **9**, 349–365

49. Hodges, B. D. M., and Wu, C. C. (2010) Proteomic insights into an expanded cellular role for cytoplasmic lipid droplets. *J. Lipid Res.* **51**, 262–273

50. Pataki, C. I., Rodrigues, J., Zhang, L., Qian, J., Efron, B., Hastie, T., Elias, J. E., Levitt, M., and Kopito, R. R. (2018) Proteomic analysis of monolayer-integrated proteins on lipid droplets identifies amphipathic interfacial α-helical membrane anchors. *Proc. Natl. Acad. Sci.* **115**, E8172–E8180

51. Bersuker, K., Peterson, C. W. H. W. H., To, M., Sahl, S. J. J., Savikhin, V., Grossman, E. A. A., Nomura, D. K. K., and Olzmann, J. A. A. (2018) A proximity labeling strategy provides insights into the composition and dynamics of lipid droplet proteomes. *Dev. Cell*. **44**, 97–112

52. Du, X., Zhou, L., Aw, Y. C., Mak, H. Y., Xu, Y., Rae, J., Wang, W., Zadoorian, A., Hancock, S. E., Osborne, B., Chen, X., Wu, J. W., Turner, N., Parton, R. G., Li, P., and

1134 Yang, H. (2020) ORP5 localizes to ER-lipid droplet contacts and regulates the level of
1135 PI(4)P on lipid droplets. *J. Cell Biol.* **219**, e201905162

1136 53. Kalogirou, C., Linxweiler, J., Schmucker, P., Snaebjornsson, M. T., Schmitz, W., Wach,
1137 S., Krebs, M., Hartmann, E., Puhr, M., Müller, A., Spahn, M., Seitz, A. K., Frank, T.,
1138 Marouf, H., Büchel, G., Eckstein, M., Kübler, H., Eilers, M., Saar, M., Junker, K.,
1139 Röhrig, F., Kneitz, B., Rosenfeldt, M. T., and Schulze, A. (2021) MiR-205-driven
1140 downregulation of cholesterol biosynthesis through SQLE-inhibition identifies
1141 therapeutic vulnerability in aggressive prostate cancer. *Nat. Commun.* **12**, 5066

1142 54. Bhaskaran, K., Douglas, I., Forbes, H., dos-Santos-Silva, I., Leon, D. A., and Smeeth,
1143 L. (2014) Body-mass index and risk of 22 specific cancers: a population-based cohort
1144 study of 5·24 million UK adults. *Lancet*. **384**, 755–765

1145 55. Onstad, M. A., Schmandt, R. E., and Lu, K. H. (2016) Addressing the role of obesity in
1146 endometrial cancer risk, prevention, and treatment. *J. Clin. Oncol.* **34**, 4225–4230

1147 56. Berstein, L. M., Tchernobrovkina, A. E., Gamajunova, V. B., Kovalevskij, A. J.,
1148 Vasilyev, D. A., Chepik, O. F., Turkevitch, E. A., Tsyrlina, E. V., Maximov, S. J.,
1149 Ashrafian, L. A., and Thijssen, J. H. H. (2003) Tumor estrogen content and clinico-
1150 morphological and endocrine features of endometrial cancer. *J. Cancer Res. Clin. Oncol.*
1151 **129**, 245–249

1152 57. D'Agostino, R., and Pearson, E. S. (1973) Tests for departure from normality: empirical
1153 results for the distributions of b2 and √b1. *Biometrika*. **60**, 613–622

1154 58. Kucharzewska, P., Christianson, H. C., and Belting, M. (2015) Global profiling of
1155 metabolic adaptation to hypoxic stress in human glioblastoma cells. *PLoS One*. **10**,
1156 e0116740

1157 59. Zhu, J., Jiang, X., and Chehab, F. F. (2014) FoxO4 interacts with the sterol regulatory
1158 factor SREBP2 and the hypoxia inducible factor HIF2α at the CYP51 promoter. *J. Lipid*
1159 *Res.* **55**, 431–442

1160 60. Liu, L., Cash, T. P., Jones, R. G., Keith, B., Thompson, C. B., and Simon, M. C. (2006)
1161 Hypoxia-Induced Energy Stress Regulates mRNA Translation and Cell Growth. *Mol.*
1162 *Cell*. **21**, 521–531

1163 61. Wong, J., Quinn, C. M., Gelissen, I. C., and Brown, A. J. (2008) Endogenous 24(S),25-
1164 epoxycholesterol fine-tunes acute control of cellular cholesterol homeostasis. *J. Biol.*
1165 *Chem.* **283**, 700–707

1166 62. Scott, N. A., Sharpe, L. J., Capell-Hattam, I. M., Gullo, S. J., Luu, W., and Brown, A. J.
1167 (2020) The cholesterol synthesis enzyme lanosterol 14α-demethylase is post-
1168 translationally regulated by the E3 ubiquitin ligase MARCH6. *Biochem. J.* **477**, 541–
1169 555

1170 63. Nguyen, K. T., Lee, C.-S., Mun, S.-H., Nhung, T. T., Park, S. K., and Hwang, C.-S.
1171 (2019) N-terminal acetylation and the N-end rule pathway control degradation of the
1172 lipid droplet protein PLIN2. *J. Biol. Chem.* **294**, 379–388

1173 64. Zavacki, A. M., Arrojo E Drigo, R., Freitas, B. C. G., Chung, M., Harney, J. W., Egri,
1174 P., Wittmann, G., Fekete, C., Gereben, B., and Bianco, A. C. (2009) The E3 ubiquitin

1175 ligase TEB4 mediates degradation of type 2 iodothyronine deiodinase. *Mol. Cell. Biol.*
1176 **29**, 5339–47

1177 65. Simonides, W. S., Mulcahey, M. A., Redout, E. M., Muller, A., Zuidwijk, M. J., Visser,
1178 T. J., Wassen, F. W. J. S., Crescenzi, A., Da-Silva, W. S., Harney, J., Engel, F. B.,
1179 Obregon, M. J., Larsen, P. R., Bianco, A. C., and Huang, S. A. (2008) Hypoxia-inducible
1180 factor induces local thyroid hormone inactivation during hypoxic-ischemic disease in
1181 rats. *J. Clin. Invest.* **118**, 975–983

1182 66. Bi, M., Naczki, C., Koritzinsky, M., Fels, D., Blais, J., Hu, N., Harding, H., Novoa, I.,
1183 Varia, M., Raleigh, J., Scheuner, D., Kaufman, R. J., Bell, J., Ron, D., Wouters, B. G.,
1184 and Koumenis, C. (2005) ER stress-regulated translation increases tolerance to extreme
1185 hypoxia and promotes tumor growth. *EMBO J.* **24**, 3470–3481

1186 67. Howe, V., Chua, N. K., Stevenson, J., and Brown, A. J. (2015) The regulatory domain
1187 of squalene monooxygenase contains a re-entrant loop and senses cholesterol via a
1188 conformational change. *J. Biol. Chem.* **290**, 27533–27544

1189 68. Olzmann, J. A., and Carvalho, P. (2019) Dynamics and functions of lipid droplets. *Nat.*
1190 *Rev. Mol. Cell Biol.* **20**, 137–155

1191 69. Yue, S., Li, J., Lee, S. Y., Lee, H. J., Shao, T., Song, B., Cheng, L., Masterson, T. A.,
1192 Liu, X., Ratliff, T. L., and Cheng, J.-X. X. (2014) Cholesteryl ester accumulation
1193 induced by PTEN loss and PI3K/AKT activation underlies human prostate cancer
1194 aggressiveness. *Cell Metab.* **19**, 393–406

1195 70. Müllner, H., Zweytick, D., Leber, R., Turnowsky, F., and Daum, G. (2004) Targeting of
1196 proteins involved in sterol biosynthesis to lipid particles of the yeast Saccharomyces
1197 cerevisiae. *Biochim. Biophys. Acta - Biomembr.* **1663**, 9–13

1198 71. Leber, R., Landl, K., Zinser, E., Ahorn, H., Spök, A., Kohlwein, S. D., Turnowsky, F.,
1199 and Daum, G. (1998) Dual localization of squalene epoxidase, Erg1p, in yeast reflects a
1200 relationship between the endoplasmic reticulum and lipid particles. *Mol. Biol. Cell.* **9**,
1201 375–386

1202 72. Jacquier, N., Choudhary, V., Mari, M., Toulmay, A., Reggiori, F., and Schneiter, R.
1203 (2011) Lipid droplets are functionally connected to the endoplasmic reticulum in
1204 Saccharomyces cerevisiae. *J. Cell Sci.* **124**, 2424–2437

1205 73. Wilfling, F., Wang, H., Haas, J. T., Krahmer, N., Gould, T. J., Uchida, A., Cheng, J. X.,
1206 Graham, M., Christiano, R., Fröhlich, F., Liu, X., Buhman, K. K., Coleman, R. A.,
1207 Bewersdorf, J., Farese, R. V., and Walther, T. C. (2013) Triacylglycerol synthesis
1208 enzymes mediate lipid droplet growth by relocalizing from the ER to lipid droplets. *Dev.*
1209 *Cell*. **24**, 384–399

1210 74. Milla, P., Athenstaedt, K., Viola, F., Oliaro-Bosso, S., Kohlwein, S. D., Daum, G., and
1211 Balliano, G. (2002) Yeast oxidosqualene cyclase (Erg7p) is a major component of lipid
1212 particles. *J. Biol. Chem.* **277**, 2406–2412

1213 75. M'barek, K. Ben, Ajjaji, D., Chorlay, A., Vanni, S., Forêt, L., and Thiam, A. R. (2017)
1214 ER membrane phospholipids and surface tension control cellular lipid droplet formation.
1215 *Dev. Cell*. **41**, 591–604

1216 76. Liu, Y., Fang, L., and Liu, W. (2021) High SQLE expression and gene amplification
1217 correlates with poor prognosis in head and neck squamous cell carcinoma. *Cancer*
1218 *Manag. Res.* **13**, 4709–4723

1219 77. Miettinen, T. A. (1982) Diurnal variation of cholesterol precursors squalene and methyl
1220 sterols in human plasma lipoproteins. *J. Lipid Res.* **23**, 466–473

1221 78. Liu, G. C. K., Ahrens, E. H. J., Schreibman, P. H., and Crouse, J. R. (1976) Measurement
1222 of squalene in human tissues and plasma: validation and application. *J. Lipid Res.* **17**,
1223 38–45

1224 79. Goldstein, J. L., Basu, S. K., and Brown, M. S. (1983) Receptor-mediated endocytosis
1225 of low-density lipoprotein in cultured cells. *Methods Enzymol.* **98**, 241–260

1226 80. Ran, F. A., Hsu, P. D., Wright, J., Agarwala, V., Scott, D. A., and Zhang, F. (2013)
1227 Genome engineering using the CRISPR-Cas9 system. *Nat. Protoc.* **8**, 2281–2308

1228 81. Stevenson, J., Krycer, J. R., Phan, L., and Brown, A. J. (2013) A practical comparison
1229 of ligation-independent cloning techniques. *PLoS One*. **8**, e83888

1230 82. Schmittgen, T. D., and Livak, K. J. (2008) Analyzing real-time PCR data by the
1231 comparative CT method. *Nat. Protoc.* **3**, 1101–1108

1232 83. Labun, K., Montague, T. G., Krause, M., Torres Cleuren, Y. N., Tjeldnes, H., and Valen,
1233 E. (2019) CHOPCHOP v3: expanding the CRISPR web toolbox beyond genome editing.
1234 *Nucleic Acids Res.* **47**, W171–W174

1235 84. Kaakoush, N. O., Olzomer, E. M., Kosasih, M., Martin, A. R., Fargah, F., Lambie, N.,
1236 Susic, D., Hoehn, K. L., Farrell, R., and Byrne, F. L. (2022) Differences in the active
1237 endometrial microbiota across body weight and cancer in humans and mice. *Cancers*
1238 *(Basel).* **14**, 2141

1239 85. Benjamini, Y., and Hochberg, Y. (1995) Controlling the false discovery rate: a practical
1240 and powerful approach to multiple testing. *J. R. Stat. Soc. Ser. B*. **57**, 289–300

1241 86. Coates, H. W. H. W., Chua, N. K. N. K., and Brown, A. J. A. J. (2019) Consulting
1242 prostate cancer cohort data uncovers transcriptional control: regulation of the MARCH6
1243 gene. *Biochim. Biophys. Acta - Mol. Cell Biol. Lipids*. **1864**, 1656–1668

1244 87. Wong, J., Quinn, C. M., and Brown, A. J. (2007) Synthesis of the oxysterol, 24(S), 25-
1245 epoxycholesterol, parallels cholesterol production and may protect against cellular
1246 accumulation of newly-synthesized cholesterol. *Lipids Health Dis.* **6**, 10

1247

1248 # Supplementary tables

1249 **Supplementary Table S1. siRNA and plasmids used for transfection**

siRNA	Description
SIC001	MISSION® universal negative control #1
SASI_Hs01_00105239	Targets human *MARCHF6* (NM_005885)
SASI_Hs01_00332063	Targets human *HIF1A* (NM_001530)
SASI_Hs01_00019152	Targets human *EPAS1* (*HIF2A*) (NM_001430)
SASI_Hs01_00016727	Targets human *HIF1AN* (*FIH-1*) (NM_017902)
Plasmid	**Description**
pCMV-$(HA)_3$-SM-V5	pcDNA3.1/V5-His TOPO vector containing the coding sequence of human squalene monooxygenase (SM; NM_003129.4) fused with three N-terminal HA epitope tags and C-terminal V5 and 6×His epitope tags, under the transcriptional control of a constitutive cytomegalovirus (CMV) promoter. Generated previously [9].
pCMV-$(HA)_3$-SM-V5 K82/90/100R	pCMV-$(HA)_3$-SM-V5 containing SM K82R, K90R and K100R substitutions, which blunt SM truncation [9]. Generated previously [9].
pCMV-$(HA)_3$-SM-V5 K290R	pCMV-$(HA)_3$-SM-V5 containing a K290R substitution, which disrupts a known ubiquitination site [32]. Generated during this study.
pCMV-$(HA)_3$-SM-V5 SM-N100 C/S/T>A	pCMV-(HA)3-SM-V5 containing SM T3A, T9A, T11A, S43A, C46A, S59A, S61A, S67A, S71A, S83A and S87A substitutions, which blunt cholesterol-induced degradation of SM [33]. Generated previously [9].
pCMV-$(HA)_3$-SM-V5 Y195F	pCMV-$(HA)_3$-SM-V5 containing an SM Y195F substitution that causes loss of catalytic activity [44]. Generated previously [9].
pCMV-SM(ΔN65)-V5	pCMV-$(HA)_3$-SM-V5 containing a deletion of the N-terminal $(HA)_3$ tag and first 65 residues of SM, which are lost upon truncation [9]. Generated previously [9].
pCMV-SM(ΔN65)-V5 Y195F	pCMV-SM(ΔN65)-V5 containing an SM Y195F substitution that causes loss of catalytic activity [44]. Generated during this study.
pCMV-GFP-ORP5	pEGFP-C1 vector containing the coding sequence of oxysterol binding protein-related protein-5 (ORP5) fused with an N-terminal GFP, under the transcriptional control of a constitutive CMV promoter. Generated previously [52].
pCMV-$(HA)_3$-SM-V5 Δ81–120	pCMV-$(HA)_3$-SM-V5 containing a deletion of SM residues 81–120, which are required for truncation [9]. Generated previously [9].
pCMV-SM-N100-GFP-V5	pcDNA3.1/V5-His TOPO vector containing the coding sequence of the first one hundred amino acids of human SM (SM-N100; NM_003129.4) fused with green fluorescent protein (GFP) and C-terminal V5 and 6×His epitope tags, under the transcriptional control of a constitutive CMV promoter. Generated previously [4].

1250

1251 **Supplementary Table S2. Primers used for qRT-PCR and DNA cloning**

1252 Non-annealing nucleotides for restriction enzyme cloning and DNA substitution are indicated
1253 in lowercase.

qRT-PCR primer pair		**Primer sequence (5′–3′)**	**Source**
VEGF	Forward Reverse	CCTGGTGGACATCTTCCAGG CTGTAGGAAGCTCATCTCTCC	[86]
CA9	Forward Reverse	GTGCCTATGAGCAGTTGCTGTC AAGTAGCGGCTGAAGTCAGAGG	Origene
RPL11	Forward Reverse	AGAGTGGAGACAGACTGACGCG CGGATGCCAAAGGATCTGACAG	Origene
GAPDH	Forward Reverse	GTCTCCTCTGACTTCAACAGCG ACCACCCTGTTGCTGTAGCCAA	Origene
ACTB	Forward Reverse	CACCATTGGCAATGAGCGGTTC AGGTCTTTGCGGATGTCCACGT	Origene
HIF1A	Forward Reverse	CAGTAACCAACCTCAGTGTGG CAGATGATCAGAGTCCAAAGC	Dr Laura Sharpe (Brown laboratory)
EPAS1 (*HIF2A*)	Forward Reverse	CTGTGTCTGAGAAGAGTAACTTCC TTGCCATAGGCTGAGGACTCCT	Origene
SQLE	Forward Reverse	GCTTCCTTCCTCCTTCATCAGTG GCAACAGTCATTCCTCCACCA	[9]
HMGCR	Forward Reverse	TTGGTGATGGGAGCTTGCTGTG AGTCACAAGCACGTGGAAGACG	[87]
HIF1AN (*FIH-1*)	Forward Reverse	CCTCTAACCTGCTGCTCATTGG GTAGAGGCACTCGAACTGATCC	Origene
DNA cloning primer pair		**Primer sequence (5′–3′)**	**Method**
SQLE gRNA 1 (promoter)	Forward Reverse	caccgAATGGAAACGTTCCGACCCG aaacCGGGTCGGAACGTTTCCATTc	*BbsI* cloning into PX598 vector (as in [80])
SQLE gRNA 2 (exon 1)	Forward Reverse	aaacAGTTCGCCCTCTTCTCGGATc caccgATCCGAGAAGAGGGCGAACT	
SM K290R	Forward Reverse	GATGGGCTTTTCTCCAgGTTCAGGAAAAGCCTG GCGATGCAATTTCCTCATTT	OEC (overlap extension cloning) [81]
SM Y195F	Forward Reverse	CCAGGTTGTAAATGGTTtCATGATTCATGATCAG G GCGATGCAATTTCCTCATTT	

1254